Please cite this article in press as: Guo et al., A Cellular System that Degrades Misfolded Proteins and Protects against Neurodegeneration, Molecular Cell (2014), http://dx.doi.org/10.1016/j.molcel.2014.04.030

Molecular Cell
Article

A Cellular System that Degrades Misfolded Proteins and Protects against Neurodegeneration

Lili Guo,[1] Benoit I. Giasson,[2,5] Alex Glavis-Bloom,[1] Michael D. Brewer,[1] James Shorter,[3] Aaron D. Gitler,[4,6] and Xiaolu Yang[1,*]
[1]Department of Cancer Biology and Abramson Family Cancer Research Institute
[2]Department of Pharmacology
[3]Department of Biochemistry and Biophysics
[4]Department of Cell and Developmental Biology
Perelman School of Medicine, University of Pennsylvania, Philadelphia, PA 19104, USA
[5]Present address: Center for Translational Research in Neurodegenerative Disease and Department of Neuroscience, University of Florida, Gainesville, FL 32610, USA
[6]Present address: Department of Genetics, Stanford University School of Medicine, Stanford, CA 94305, USA
*Correspondence: xyang@mail.med.upenn.edu
http://dx.doi.org/10.1016/j.molcel.2014.04.030

SUMMARY

Misfolded proteins compromise cellular function and cause disease. How these proteins are detected and degraded is not well understood. Here we show that PML/TRIM19 and the SUMO-dependent ubiquitin ligase RNF4 act together to promote the degradation of misfolded proteins in the mammalian cell nucleus. PML selectively interacts with misfolded proteins through distinct substrate recognition sites and conjugates these proteins with the small ubiquitin-like modifiers (SUMOs) through its SUMO ligase activity. SUMOylated misfolded proteins are then recognized and ubiquitinated by RNF4 and are subsequently targeted for proteasomal degradation. We further show that PML deficiency exacerbates polyglutamine (polyQ) disease in a mouse model of spinocerebellar ataxia 1 (SCA1). These findings reveal a mammalian system that removes misfolded proteins through sequential SUMOylation and ubiquitination and define its role in protection against protein-misfolding diseases.

INTRODUCTION

Proteins are the most abundant macromolecules of the cell and are critical to virtually all physiological processes. To perform their biological functions, the majority of proteins need to fold into and maintain their native conformations. Although the native conformation of a protein is determined by its amino acid sequence, the folding process is extraordinarily complex and highly prone to error, and its utility can be further limited in situations of genetic mutations, biogenetic inaccuracies, and posttranslational damages (Dobson, 2003; Goldberg, 2003). Proteins that have adopted aberrant conformations, and the aggregates formed by them, pose a constant threat to cell viability and function. Failure to eliminate these proteins is closely linked to the pathogenesis of various debilitating human diseases (Selkoe, 2003; Taylor et al., 2002).

To contend with protein misfolding, cells employ two broad sets of protein quality control (PQC) systems: systems that assist proteins in achieving their native conformations, and systems that eliminate misfolded proteins once they are formed. The former consist mainly of a large number of molecular chaperones and their cochaperones, which in an ATP-dependent manner protect proteins in their nonnative state and reduce misfolding and aggregation. Notable examples include (1) heat shock protein 70 (Hsp70), which aids the folding of a wide range of proteins; (2) Hsp60/chaperonin, which forms a macromolecular cage to encapsulate relatively small proteins for uninterrupted folding; and (3) HSP90, which most commonly acts on proteins involved in cell signaling and transcription (Hartl et al., 2011).

Systems that remove misfolded proteins include protein disaggregases. Especially, Hsp100 proteins in prokaryotes or lower eukaryotes (e.g., ClpB in bacteria and Hsp104 in yeast) can resolubilize protein aggregates, functioning in concert with Hsp70 and its cochaperone Hsp40 (Glover and Lindquist, 1998). Nevertheless, given that protein misfolding is inevitable and often cannot be reversed due to mutations, biogenetic errors, or irreparable damages, cells ultimately rely on degradative systems to maintain protein quality. Yet, these systems are still poorly understood. Although the ubiquitin-proteasome pathway, along with autophagy, must be an important part of these systems, the critical issue of how they selectively recognize misfolded proteins and target them for degradation remains elusive (Goldberg, 2003; Tyedmers et al., 2010).

Furthermore, compared to the other cellular compartments such as the endoplasmic reticulum (Buchberger et al., 2010), the PQC systems in the nucleus are conspicuously unclear. Misfolded proteins in the nucleus can be particularly damaging to postmitotic mammalian cells (e.g., neurons and cardiac myocytes), which are unable to remove these proteins through the breakdown of the nuclear envelope during mitosis. The importance of understanding PQC in this cellular compartment is emphasized by the formation of neuronal intranuclear inclusions that are associated with various dominantly inherited neurodegenerative diseases, including Huntington's disease (HD) and

Please cite this article in press as: Guo et al., A Cellular System that Degrades Misfolded Proteins and Protects against Neurodegeneration, Molecular Cell (2014), http://dx.doi.org/10.1016/j.molcel.2014.04.030

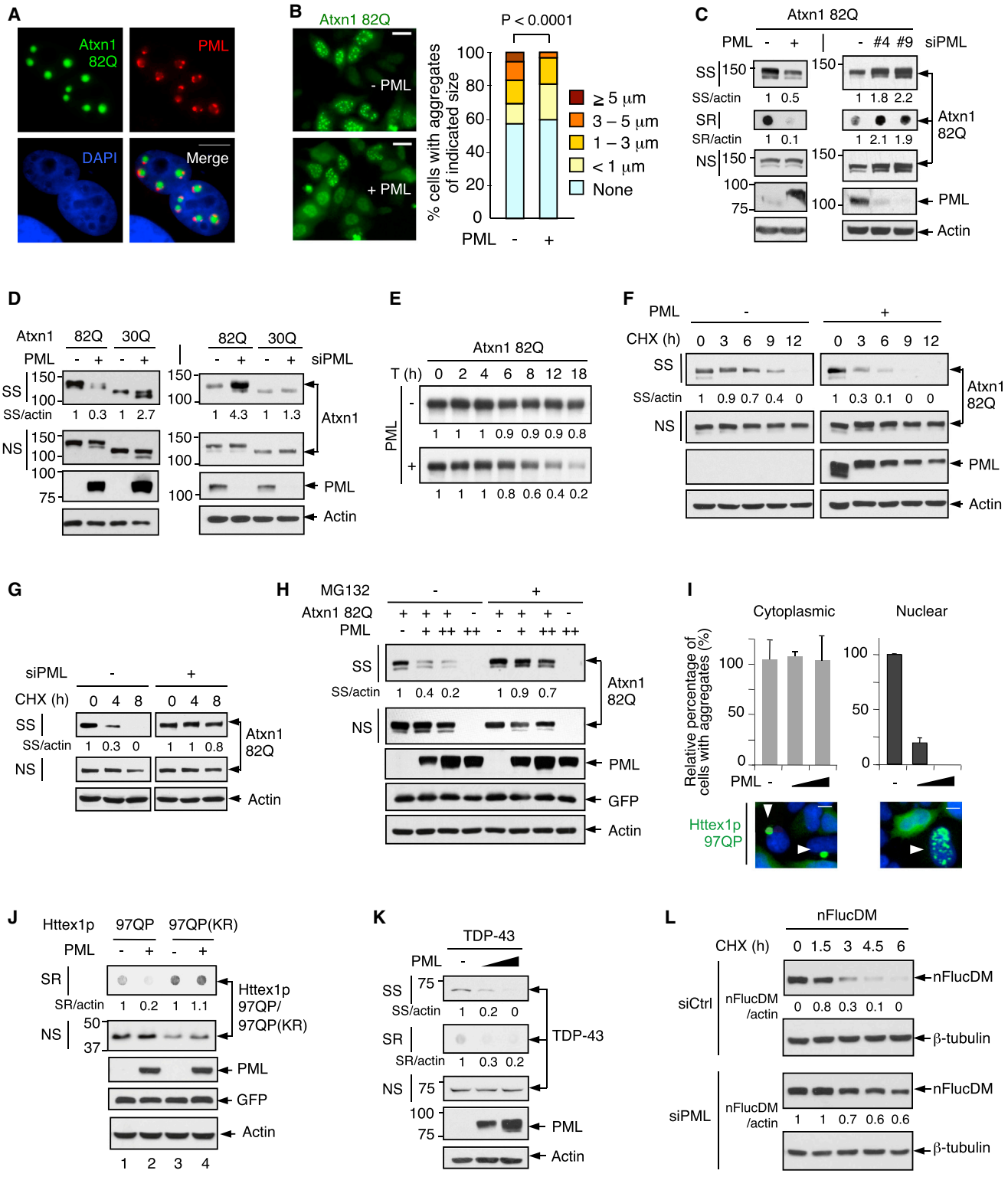

Figure 1. PML Promotes the Degradation of Atxn1 82Q and Other Nuclear Misfolded Proteins

(A) HeLa cells transfected with Atxn1 82Q-GFP were stained with anti-PML antibody (red) and DAPI (blue). Individual and merged images are shown. Scale bar, 10 μm.

(B) Atxn1 82Q-GFP was expressed alone or together with PML in HeLa cells. Left, representative fluorescence images of cells. Scale bar, 20 μm. Right, quantification of cells based on sizes of Atxn1 82Q-GFP inclusions.

(legend continued on next page)

several types of spinocerebellar ataxias (SCAs). These diseases are caused by an expansion within the relevant genes of a CAG repeat, which encodes a polyQ stretch. They are manifested when the polyQ stretch exceeds a threshold length that is disease specific, and become progressively more severe as its length increases (Orr and Zoghbi, 2007).

The promyelocytic leukemia protein (PML; also known as TRIM19) is a member of the tripartite motif (TRIM) family of proteins, which contain an N-terminal TRIM/BRCC region, consisting of a RING domain, one or two B boxes, and a coiled-coil (CC) motif, followed by a variable C-terminal region. PML is predominantly a nuclear protein and is the eponymous component of PML nuclear bodies. It is implicated in a wide variety of cell processes, including apoptosis, transcription, DNA damage signaling, and antiviral responses (Bernardi and Pandolfi, 2007). Notably, PML also colocalizes with aggregates formed by polyQ proteins associated with SCAs (Skinner et al., 1997; Takahashi et al., 2003) and, upon overexpression, promotes degradation of at least one of them (mutant ataxin-7) (Janer et al., 2006). Despite the potential importance of these observations, the role of PML in the removal of misfolded proteins is not well understood. In particular, it is unclear whether PML plays a broad role in the removal of nuclear misfolded proteins. The critical issue of the molecular mechanisms by which PML removes misfolded proteins is unaddressed. Moreover, the physiological relevance of the effect of PML on misfolded proteins is not known. We set out to investigate these issues in the current study.

RESULTS

PML Promotes Proteasomal Degradation of Pathogenic Ataxin-1 Protein

SCA1 is a fatal neurological disorder characterized by progressive ataxia and loss of neurons, especially cerebellar Purkinje cells. It is caused by the expansion of a polyQ stretch in the *SCA1* gene product, Ataxin-1 (Atxn1) (Orr and Zoghbi, 2007). To investigate the role of PML in eliminating nuclear misfolded proteins, we generated a cell culture model in which a pathogenic Atxn1 protein with 82 contiguous glutamines that was C-terminally fused to the enhanced green fluorescent protein, Atxn1 82Q-GFP, was expressed in HeLa cells. Similar to pathogenic Atxn1 proteins in human SCA1 patients and mouse SCA1 transgenic models (Skinner et al., 1997), Atxn1 82Q-GFP was localized to the nucleus, exhibiting a diffuse localization pattern with markedly higher concentration in microscopically visible inclusions (Figures 1A and 1B). Atxn1 82Q-GFP also yielded both NP-40-soluble (soluble or NS) and NP-40-insoluble (aggregated) species in cell lysates. The latter could be further divided into SDS-soluble (SS) and SDS-resistant (SR) species (Figure 1C).

Concordant with previous reports (Skinner et al., 1997), endogenous PML colocalized with Atxn1 82Q-GFP inclusions, accumulating in bodies adjacent to them and also being distributed within (Figure 1A). PML is expressed as several isoforms (Nisole et al., 2013). We examined five major PML isoforms (I, II, III, IV, and VI) and found that all five colocalized with Atxn1-GFP inclusions (see Figure S1A online). For subsequent analyses, we chose the commonly used isoform IV (hereafter called PML unless otherwise noted).

When coexpressed with Atxn1 82Q, PML significantly decreased the size of Atxn1 82Q-GFP nuclear inclusions (Figure 1B). It also reduced the steady-state levels of the Atxn1 82Q-GFP protein, especially the aggregated SS and SR species (Figure 1C, left). To evaluate the effect of endogenous PML (all isoforms), we knocked it down using two independent small interfering RNAs (siRNAs). This noticeably raised the levels of Atxn1 82Q-GFP, especially aggregated species (Figure 1C, right). Silencing PML also increased the steady-state levels of a FLAG-tagged Atxn1 82Q protein (Figure S1B). The effect of PML siRNA on Atxn1 82Q could be reversed by an siRNA-resistant form of PML (Figure S1C), ruling out off-target effects of the siRNA.

To evaluate whether PML specifically reduces pathogenic Atxn1 proteins, we used a nonpathogenic ataxin-1 protein, Atxn1 30Q. Forced expression of PML did not reduce the abundance of Atxn1 30Q-GFP, while knockdown of PML did not significantly augment it either (Figure 1D), underscoring the selective effect of PML on pathogenic Atxn1 proteins.

PML did not inhibit the transcription of the *Atxn1 82Q* gene (Figure S1D). To determine whether PML promotes the degradation of the Atxn1 82Q protein, we performed a pulse-chase assay. In the absence of cotransfected PML, total [^{35}S]-labeled Atxn1 82Q protein was rather stable, and its levels declined only ~20% in 18 hr. By contrast, in the presence of PML, total

(C) Atxn1 82Q-GFP was expressed alone or together with PML in HeLa cells (left), or alone in HeLa cells that were previously treated with control (−) or PML siRNA. Cell lysate fractions (when indicated) and whole-cell lysates (WCL) were analyzed by filter retardation assay (for SR fraction) or western blot (WB; for the rest). Molecular weight standards (in kDa) and relative ratios of SS or SR Atxn1 versus actin are indicated.

(D) Steady-state levels of FLAG-Atxn1 82Q or 30Q when expressed alone or together with PML in HeLa cells (left), or when expressed alone in HeLa cells that were treated with control or PML siRNA (right), analyzed by WB.

(E) Effect of PML on the stability of total FLAG-Atxn1 82Q protein, analyzed by a pulse-chase assay and autoradiography. The relative amounts of ^{35}S-labeled Atxn1 82Q are indicated.

(F and G) Effect of PML overexpression (F) and knockdown (G) on the stability of Atxn1 82Q-GFP, analyzed by CHX treatment and WB.

(H) Effect of PML on Atxn1 82Q-GFP levels in the absence or presence of MG132.

(I) Top, relative percentages of Httex1p 97QP-expressing cells with cytoplasmic (left) and nuclear (right) inclusions, in the absence or presence of PML (means + SD, n = 3). Bottom, representative fluorescence images of transfected cells immunostained with an anti-Htt antibody. Arrowheads indicate Httex1p 97QP aggregates.

(J and K) Levels of HA-Httex1p 97QP and HA-Httex1p 97QP(KR) (J) and GFP-TDP-43 (K) in cells with and without PML overexpression. Virtually all Htt aggregates were in the SR fraction.

(L) Stability of nFucDM-GFP in control and PML-depleted cells, analyzed by CHX treatment and WB.

See also Figure S1.

Please cite this article in press as: Guo et al., A Cellular System that Degrades Misfolded Proteins and Protects against Neurodegeneration, Molecular Cell (2014), http://dx.doi.org/10.1016/j.molcel.2014.04.030

[^{35}S]Atxn1 82Q protein was destabilized, and its levels declined ~80% over the same period of time (Figure 1E).

We also used cycloheximide (CHX) to block protein synthesis and examined the degradation of the pre-existing Atxn1 82Q protein. Forced expression of PML accelerated the degradation of aggregated Atxn1 82Q, reducing its half-life from ~8 hr to ~2 hr, while having a minimal effect on soluble Atxn1 82Q (Figure 1F). Conversely, silencing PML prolonged the half-life of aggregated Atxn1 82Q and, to a lesser extent, the half-life of soluble Atxn1 82Q (Figure 1G). The ability of PML to remove aggregated Atxn1 82Q was markedly diminished by the proteasome inhibitor MG132 (Figure 1H). In contrast, PML did not alter the half-life of Atxn1 30Q (Figure S1E). Collectively, these results indicate that PML targets pathogenic, but not normal, Atxn1 protein for proteasomal degradation.

A General Role for PML in Degrading Nuclear Misfolded Proteins

To assess whether PML plays a broad role in degrading misfolded proteins in the nucleus, we tested two additional proteins linked to neurodegeneration: (1) a pathogenic fragment of huntingtin (Htt) encoded by the first exon of the *HD* gene, Httex1p 97QP (Steffan et al., 2004); and (2) TAR DNA-binding protein 43 (TDP-43), which is associated with both amyotrophic lateral sclerosis (ALS, also known as Lou Gehrig's disease) and frontotemporal lobar degeneration with ubiquitinated inclusions (FTLD-U) (Chen-Plotkin et al., 2010). Httex1p 97QP formed microscopically visible inclusions in both the nucleus and the cytoplasm (Figure 1I), while TDP-43 formed inclusions mainly in the nucleus (data not shown). PML reduced the nuclear, but not the cytoplasmic, Httex1p 97QP inclusions (Figure 1I), and decreased the amount of aggregated Httex1p 97QP (Figure 1J, lanes 1 and 2). PML also lowered the amount of aggregated, but not soluble, TDP-43 (Figure 1K).

To extend these analyses, we used a structurally destabilized mutant of the model chaperone substrate firefly luciferase (FlucDM), which was developed as a probe for the capacity of cellular PQC systems (Gupta et al., 2011). Endogenous PML partially colocalized with a nuclear form of FlucDM (nFlucDM-GFP), which formed inclusions, but not with the wild-type counterpart (nFlucWT-GFP), which displayed diffuse localization (Figure S1F). Silencing PML noticeably elevated the levels of aggregated nFlucDM-GFP (Figure S1G) and extended the half-life of total nFlucDM-GFP protein (Figure 1L). Taken together, these results indicate that PML facilitates the removal of multiple misfolded proteins in the mammalian cell nucleus.

Recognition of Misfolded Proteins by Distinct Sites on PML

To investigate the mechanism by which PML degrades misfolded proteins, we first examined whether PML is able to directly recognize these proteins. We used a pathogenic (103Q) and a nonpathogenic (25Q) Htt fragment, each being fused to glutathione S-transferase (GST). In an in vitro assay with purified recombinant proteins, immobilized FLAG-PML, but not the control protein FLAG-GFP, pulled down GST-Htt 103Q (Figure 2A), indicating a specific and direct interaction between PML and Htt 103Q. FLAG-PML also pulled down GST-Htt 25Q. However, this interaction was substantially weaker than the PML-Htt 103Q interaction (Figure 2A). In a reciprocal experiment, immobilized GST-Htt 103Q proteins also interacted more strongly with FLAG-PML than immobilized GST-Htt 25Q did (Figure S2A). Hsp70 and Hsp40, which recognize a broad range of misfolded proteins, did not enhance the PML-Htt 103Q interaction (Figure 2A). These results suggest that PML can directly associate with polyQ proteins and preferentially with the pathogenic form.

We also examined whether PML selectively binds to denatured luciferase. 6xHis-tagged luciferase that was immobilized on Ni-NTA beads was either denatured with urea or kept in the native form. Denatured, but not native, luciferase specifically interacted with GST-PML, and the Hsp70/Hsp40 system did not enhance this interaction (Figure 2B). Thus, PML can directly recognize misfolded, but not native, luciferase.

To understand the molecular basis for the interaction of PML with misfolded proteins, we sought to identify the substrate recognition sites (SRSs) of PML, as well as the structural features on substrates that these SRSs discern. It was previously shown that, in a manner dependent on its length, polyQ and the flanking regions form CC structures, which facilitate the assembly of polyQ proteins into an oligomeric or aggregated state and also mediate the interaction of polyQ proteins with CC-containing proteins (Fiumara et al., 2010). This led us to hypothesize that PML, via its CC region within the TRIM/RBCC motif, might interact with pathogenic polyQ proteins. We constructed a panel of PML fragments (F1–F5) that either contained or lacked the CC region (Figure S2B). A fragment containing the CC region (F1) interacted with Htt 103Q, while two fragments lacking this region (F2 and F3) did not (Figures S2B and S2C). Moreover, the CC region alone (F4) bound to Htt 103Q, while deleting this region from the entire PML protein (F5 or ΔCC) greatly diminished this binding. Thus, PML recognizes Htt 103Q almost exclusively through the CC region. Similar to the full-length PML, PML CC displayed a clear binding preference for the pathogenic Htt 103Q to the nonpathogenic Htt 25Q (Figure 2C). PML CC also strongly interacted with another pathogenic Htt construct, Htt 52Q (Figure 2C). Thus, PML CC likely constitutes an SRS (called SRS1).

To test whether PML CC recognizes the homologous CC structure in Htt proteins, we mutated the residues in Htt 52Q that were predicted to be involved in the CC formation, yielding Htt 52Q cc- (Figure S2D). A similar mutation was previously shown to reduce the formation of the CC structure in Htt 72Q (Fiumara et al., 2010). Indeed, compared to Htt 52Q, Htt 52Q cc- displayed a noticeably reduced propensity to form aggregates (data not shown) and a substantially weaker interaction with PML CC (Figure 2C). Therefore, PML CC/SRS1 likely interacts with the CC structure on pathogenic Htt proteins.

Given that PML also promotes the degradation of non-polyQ proteins such as luciferase and TDP-43 (Figures 1 and S1), we reasoned that PML might contain at least another SRS that could discern non-CC structural features on misfolded proteins. To test this possibility, we examined the panel of PML fragments for interaction with denatured luciferase. Although the CC region alone could interact with denatured luciferase, significant levels of interaction were also observed in two fragments (F2 and F5) that lacked this region but contained the C terminus

Please cite this article in press as: Guo et al., A Cellular System that Degrades Misfolded Proteins and Protects against Neurodegeneration, Molecular Cell (2014), http://dx.doi.org/10.1016/j.molcel.2014.04.030

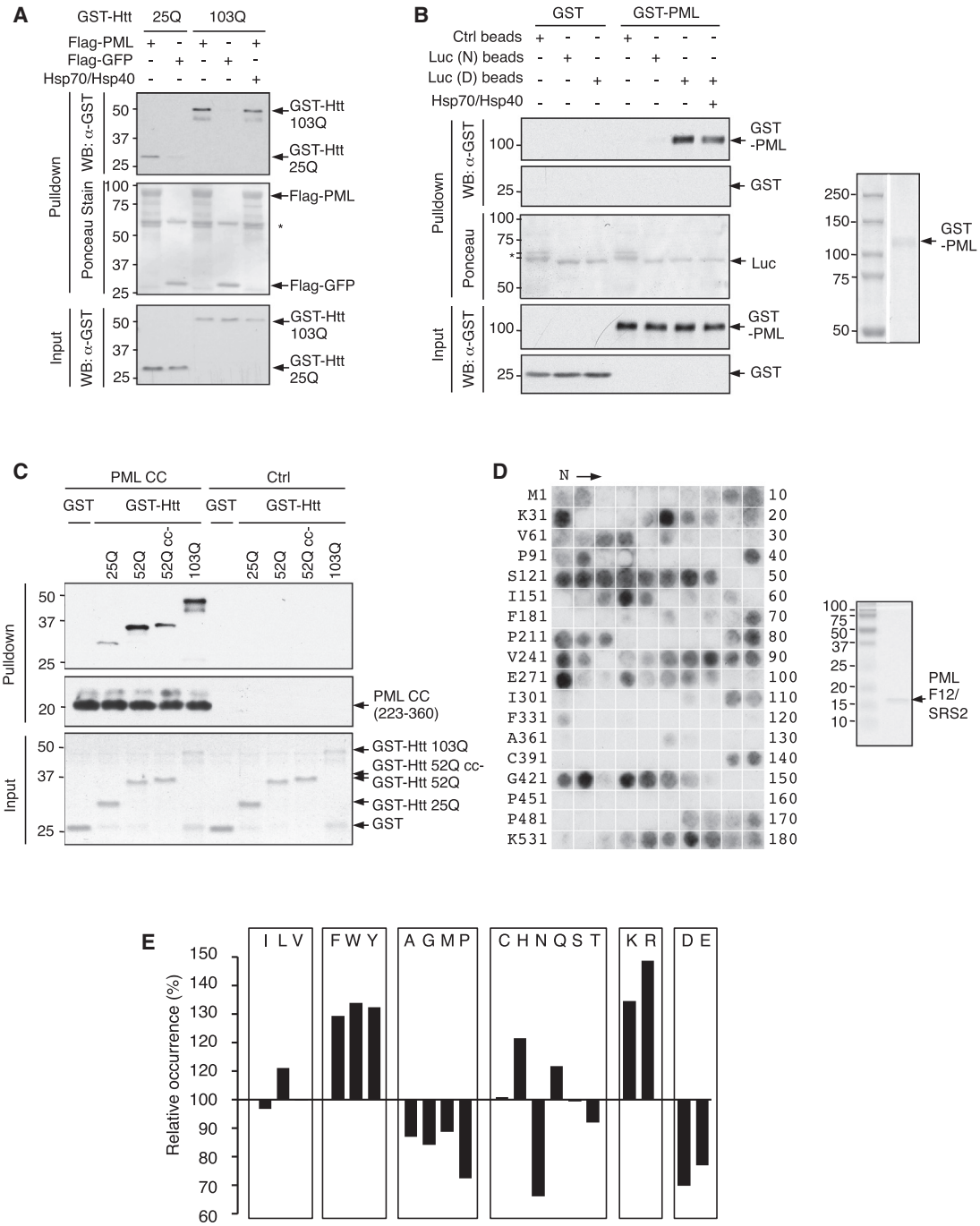

Figure 2. Recognition of Misfolded Proteins by PML

(A) Binding of GST-Htt 25Q and GST-Htt 103Q to immobilized FLAG-PML and FLAG-GFP (negative control), analyzed by an in vitro pull-down assay followed by WB (top and bottom) and Ponceau S staining (middle). *IgG heavy chain.

(B) Binding of GST-PML (shown on the right) and the control GST protein to native (N) and urea-denatured (D) luciferase (luc) immobilized on Ni-NTA beads, analyzed as in (A). *Nonspecific proteins from BL21 bacterial lysates that bound to the control beads.

(C) Binding of indicated GST-Htt fusions to FLAG-PML CC conjugated on anti-Flag M2 beads or to control beads, analyzed by WB (top and middle) and Coomassie staining (bottom).

(D) Binding of PML F12/SRS2 (shown on the right) to a peptide library derived from luciferase. The N-terminal amino acid of the first peptide and the number of the last peptide spotted in each row are indicated.

(E) The occurrence of each amino acid in PML SRS2-binding peptides relative to its occurrence in the luciferase peptide array (set at 100%).

See also Figures S2 and S3.

Please cite this article in press as: Guo et al., A Cellular System that Degrades Misfolded Proteins and Protects against Neurodegeneration, Molecular Cell (2014), http://dx.doi.org/10.1016/j.molcel.2014.04.030

(aa 361–633) (Figures S2B and S3A). Using additional deletion constructs within the C terminus (F6–F18, Figures S2B and S3B), we found that a stretch of 63 amino acids (aa 571–633) was sufficient for binding to denatured luciferase. Either NH_2- or COOH-terminal deletions of this stretch abolished the binding (Figure S3). Thus, the last 63 amino acids of PML likely constitute another SRS (called SRS2).

To investigate the linear sequences in luciferase that can be recognized by PML SRS2, we used purified PML SRS2 to screen a cellulose-bound peptide library that represented the complete sequence of luciferase. The library consisted of 180 peptides, each containing 13 amino acid residues that overlapped adjacent peptides by ten. Similar to chaperones such as Hsp70 and ClpB (Rüdiger et al., 1997; Schlieker et al., 2004), PML SRS2 only bound to a subset of these peptides (Figure 2D), indicating its ability to distinguish peptides with different amino acid compositions. An analysis of the relative occurrence of all 20 amino acids in PML SRS2-interacting peptides versus all peptides in the library showed that PML SRS2 strongly favored aromatic (Phe, Trp, and Tyr) and positively charged (Arg and Lys) residues, and disfavored negatively charged residues (Asp and Glu) (Figure 2E). This amino acid preference was similar to that of ClpB, except that SRS2 had an additional preference for Leu and His, which are disfavored by ClpB (Schlieker et al., 2004).

For comparison, we tested the binding of PML CC/SRS1 to the peptide library. Consistent with the notion that this region recognizes higher-order structures instead of linear sequences, PML CC/SRS1 weakly bound to only a few peptides (Figure S2E). Based on these results, we conclude that PML contains at least two regions that can recognize misfolded proteins: the CC region within the TRIM/RBCC motif (SRS1) and the 63 amino acid stretch at its C terminus (SRS2), which can discern CC structures and exposed peptides enriched in both aromatic and basic amino acids, respectively.

Involvement of SUMOylation in the Degradation of Atxn1 82Q

How might PML promote the degradation of misfolded proteins upon recognition? Misfolded proteins associated with neurodegeneration are frequently modified by SUMO, although the role of this modification remains unclear (Martin et al., 2007). Mammalian cells express three major SUMO proteins, SUMO1–SUMO3. SUMO2 and SUMO3 are nearly identical to each other in their sequence (collectively called SUMO2/3) and are approximately 50% identical to SUMO1 (Wilkinson and Henley, 2010). We investigated the modification of Atxn1 82Q by these SUMO proteins and their involvement in Atxn1 82Q degradation.

Atxn1 82Q was modified by both exogenous (Riley et al., 2005) and endogenous (Figure 3A, left) SUMO1, and this modification was weaker than that of Atxn1 30Q (Riley et al., 2005). Atxn1 82Q was also modified by endogenous SUMO2/3 (Figure 3A, right), and colocalized with GFP-SUMO2/3 in the nucleus (Figure 3B). The sites in Atxn1 82Q that were conjugated with SUMO1 and SUMO2/3 might be different, because a mutant Atxn1 82Q with impaired SUMO1 conjugation, Atxn1 82Q (5KR) (Riley et al., 2005), showed no defect in SUMO2/3 conjugation (Figure S4A).

Of note, Atxn1 82Q was more strongly modified by endogenous SUMO2/3 compared to Atxn1 30Q (Figure 3C), correlating with the different responses of these Atxn1 proteins to PML-mediated degradation (Figures 1 and S1). Similarly, TDP-43 was modified by endogenous SUMO2/3 (Figure S4B). So was FlucDM, as well as another structurally destabilized luciferase mutant, FlucSM (Gupta et al., 2011). The SUMO2/3 modification of these luciferase mutants was also stronger than that of wild-type luciferase (Figure S4C).

Moreover, proteasome inhibition enhanced the colocalization of Atxn1 82Q with GFP-SUMO2/3 (Figure 3B). It also increased SUMO2/3-modified Atxn1 82Q concurrently with ubiquitinated Atxn1 82Q, but not SUMO1-modified Atxn1 82Q (Figure 3A and Figure 3D, lanes 2 and 3). Likewise, proteasome inhibition increased SUMO2/3-modified TDP-43 and luciferase mutants (Figures S4B and S4C).

To assess the role of SUMO proteins in the ubiquitination and proteasomal degradation of Atxn1 82Q, we silenced SUMO2/3 and SUMO1 separately using siRNA. Silencing SUMO2/3, but not SUMO1, effectively reduced ubiquitination of Atxn1 82Q (Figure 3D, lanes 4–7). Silencing SUMO2/3 also raised the levels of Atxn1 82Q, especially the aggregated form, but not the levels of the control protein GFP (Figures S4D–S4F), and it diminished the ability of PML to remove aggregated Atxn1 82Q (Figure 3E).

SUMO2 and SUMO3 contain an internal SUMOylation consensus site that enables the formation of polychains. SUMO1 does not contain this site, and when conjugated to the SUMO2/3 chain, it can terminate the chain elongation (Wilkinson and Henley, 2010). Therefore, we used two additional strategies to inhibit the modification of Atxn1 82Q by SUMO2/3. First, we overexpressed SUMO1. This strongly reduced Atxn1 82Q conjugation to SUMO2/3 and, at the same time, impaired conjugation of Atxn1 82Q to ubiquitin (Figure 3D, lanes 8 and 9) and its degradation by PML (Figure 3F, left). Second, we used a SUMO2 mutant that was deficient in chain formation, SUMO2 KR. Overexpression of SUMO2 KR effectively reduced the amount of SUMO2/3-modified Atxn1 82Q species, especially those of high molecular weights. It also reduced ubiquitin-modified Atxn1 82Q species (Figure 3D, lanes 12 and 13) and blunted the ability of PML to degrade Atxn1 82Q (Figure 3F, right). Moreover, we used a SUMOylation-defective Htt mutant, Httex1p 97QP(KR) (Steffan et al., 2004), and found that it was resistant to the PML-mediated degradation (Figure 1J). Taken together, these results show that ubiquitination and degradation of Atxn1 82Q and likely other misfolded proteins are dependent on their modification by SUMO2/3.

PML as a SUMO E3 Ligase of Atxn1 82Q

We previously demonstrated that PML possesses SUMO E3 ligase activity that enhances the efficiency and specificity of SUMOylation (Chu and Yang, 2011). Hence, we examined whether PML promotes SUMOylation of Atxn1 82Q. When coexpressed with Atxn1 82Q in cells, PML strongly increased SUMO2/3 modification of Atxn1 82Q, both in the absence and in the presence of the proteasome inhibitor MG132 (Figure 4A). Conversely, silencing PML markedly reduced SUMO2/3-modified Atxn1 82Q under these conditions (Figure 4B). Similarly, silencing PML reduced SUMO2/3 modification of nFlucDM (Figure 4C).

To confirm the SUMO E3 activity of PML toward Atxn1 82Q, we performed in vitro SUMOylation assays with purified recombinant

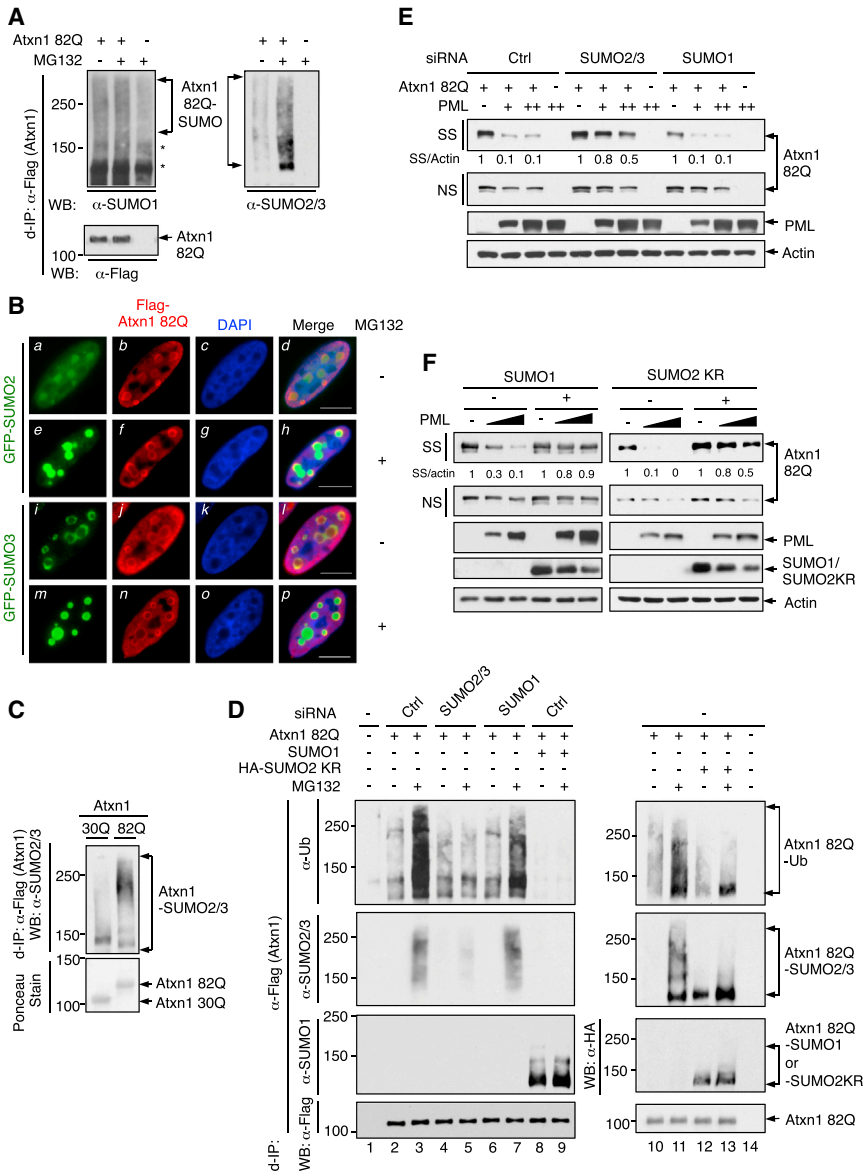

Figure 3. SUMO2/3 Is Involved in the Ubiquitination and PML-Mediated Degradation of Atxn1 82Q

(A) SUMO1 and SUMO2/3 modification of Atxn1 82Q in HeLa cells treated without or with MG132. For better comparison of modified Atxn1 82Q, Denaturing immunoprecipitation (d-IP) products with a similar level of unmodified Atxn1 82Q were analyzed by WB. *Nonspecific bands.

(B) Localization of Atxn1 82Q (detected by anti-FLAG antibody, red) in GFP-SUMO2- or GFP-SUMO3-expressing U2OS cells treated with or without MG132. Scale bar, 10 μm.

(C) SUMO2/3 modification of Atxn1 82Q and 30Q in HeLa cells, analyzed by d-IP followed by WB (top) and Ponceau S staining (bottom).

(D) Atxn1 82Q was expressed alone or together with SUMO1 or HA-SUMO2 KR in HeLa cells that were previously transfected with the indicated siRNA or un-transfected (–). Cells were treated with or without MG132. SUMOylation and ubiquitination of FLAG-Atxn1 82Q was analyzed by d-IP and WB.

(E) Levels of Atxn1 82Q-GFP expressed alone or together with increasing amounts of PML in HeLa cells pretreated with the indicated siRNA.

(F) Effect of PML on Atxn1 82Q-GFP levels in the presence or absence of SUMO1 or SUMO2 KR. See also Figure S4.

proteins. In the absence of PML, Atxn1 82Q was weakly modified by SUMO2 (Figures 4D and 4E), consistent with previous observations that SUMOylation can proceed in vitro without a SUMO E3 ligase (Wilkinson and Henley, 2010). Of note, PML augmented Atxn1 82Q SUMOylation in a dose-dependent manner (Figures 4D and 4E). In contrast, a SUMO E3-defective mutant, PML M6 (Chu and Yang, 2011), failed to do so (Figures 4E and S4G); PML M6 was also ineffective at reducing aggregated Atxn1 82Q (Figure 4F). These results suggest that PML is a SUMO E3 ligase of Atxn1 82Q, and that this activity is involved in Atxn1 82Q degradation.

A Role for RNF4 in Degrading Misfolded Proteins

Proteins conjugated with a poly-SUMO2/3 chain can be recognized and ubiquitinated by RNF4, a RING domain ubiquitin ligase with four tandem SUMO-interacting motifs (SIMs) (Sun et al., 2007). However, the role of RNF4 in degrading misfolded proteins remains undefined. We found that forced RNF4 expression strongly reduced the steady-state levels of aggregated Atxn1 82Q in cell lysates (Figure 5A), as well as the number of Atxn1 82Q inclusions in the nucleus (Figure S5A). RNF4 also shortened the half-life of aggregated, but not soluble, Atxn1 82Q (Figure 5B, lanes 1–12; Figures 5C and S5B). Conversely, knocking down endogenous RNF4 with three siRNAs, individually or in combination, increased total and aggregated Atxn1 82Q proteins in cell lysates (Figures 5D, S5C, and S5D), as well as Atxn1 82Q inclusions in the nucleus (Figure 5E). An siRNA-resistant form of RNF4 could reverse the effect of RNF4 knockdown (Figure S5C), indicative of the specificity of the siRNA.

Moreover, both endogenous and exogenous RNF4 proteins normally displayed a diffuse nuclear distribution pattern with minimal or moderate colocalization with Atxn1 82Q inclusions. But on proteasome blockage RNF4 became highly enriched in Atxn1 82Q inclusions (Figures 5F and S5E), likely reflecting a stalled attempt of RNF4 in clearing Atxn1 82Q. In contrast to its effect on Atxn1 82Q, RNF4 did not reduce the levels of Atxn1 30Q (Figure 5G). Collectively, these results demonstrate a role for RNF4 in eliminating pathogenic Atxn1 proteins.

To assess a general effect of RNF4 on misfolded proteins, we tested it on Httex1p 97QP, TDP-43, and nFlucDM. Forced expression of RNF4 markedly reduced Httex1p 97QP, especially the aggregated form, while having a much weaker effect on Httex1p

Please cite this article in press as: Guo et al., A Cellular System that Degrades Misfolded Proteins and Protects against Neurodegeneration, Molecular Cell (2014), http://dx.doi.org/10.1016/j.molcel.2014.04.030

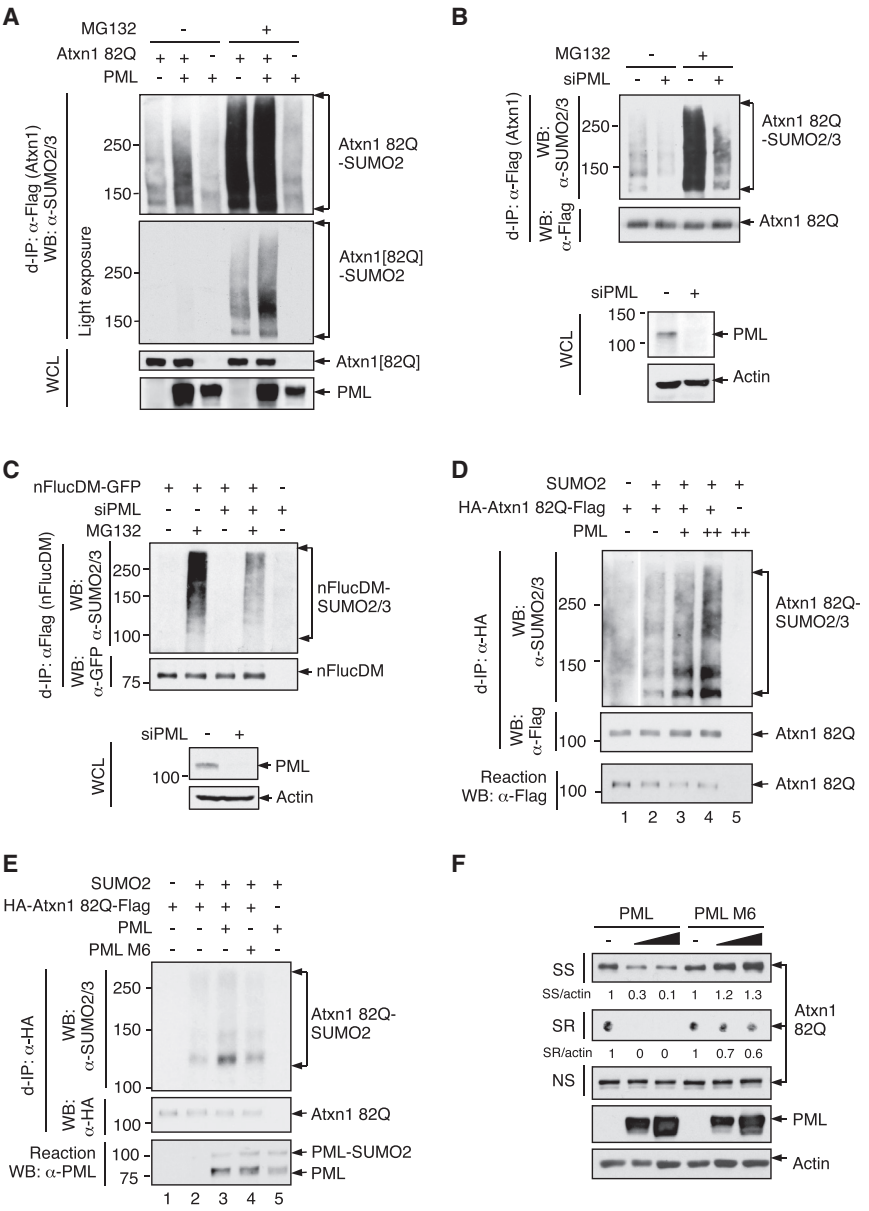

Figure 4. PML Promotes SUMOylation of Atxn1 82Q

(A) SUMOylation of FLAG-Atxn1 82Q in HeLa cells in the absence or presence of HA-PML cells, and without or with MG132 treatment. The amount of Atxn1 82Q DNA used for transfected was adjusted to yield comparable levels of the unmodified protein.

(B and C) SUMOylation of FLAG-Atxn1 82Q (B) and FLAG-nFlucDM-GFP (C) in control and PML siRNA-transfected HeLa cells treated without or with MG132.

(D and E) SUMOylation of purified HA-Atxn1 82Q-FLAG was performed in the presence of recombinant FLAG-PML, FLAG-PML M6, and SUMO2 as indicated. In (D), the amounts of different d-IP products were adjusted to yield a similar level of unmodified Atxn1 82Q (middle).

(F) Levels of Atxn1 82Q-GFP in HeLa cells in the absence or presence of increasing amounts of PML or PML M6.

See also Figure S4.

97QP(KR) (Figure 5H). Likewise, forced expression of RNF4 decreased the levels of TDP-43 (Figure S5F), whereas silencing RNF4 augmented the percentage of TDP-43-expressing cells with nuclear inclusions (Figures S5G and S5H). Upon proteasome inhibition, endogenous RNF4 became highly enriched in TDP-43 inclusions (Figure S5I), similar to its accumulation in Atxn1 82Q inclusions under the same conditions (Figure 5F). Moreover, silencing RNF4 prolonged the half-life of nFlucDM (Figure 5I). Collectively, these observations suggest that RNF4 plays a critical role in the degradation of diverse misfolded proteins.

RNF4 Mediates Ubiquitination and Degradation of SUMO2/3-Modified Atxn1 82Q

Similar to PML, the ability of RNF4 to eliminate misfolded proteins was dependent on SUMO2/3, as this ability was compromised in cells devoid of SUMO2/3, but not in cells devoid of SUMO1 (Figure S6A). Of note, forced expression of RNF4 preferentially reduced SUMO2/3-modified Atxn1 82Q and nFlucDM over the unmodified proteins (Figures 6A and 6B). Conversely, silencing RNF4 increased SUMO2/3-modified Atxn1 82Q (Figure 6C) and enhanced the colocalization of Atxn1 82Q with GFP-SUMO2 (Figure S6B). These results show that RNF4 targets SUMO2/3-modified misfolded proteins for degradation.

To confirm that RNF4 ubiquitinates SUMO2/3-conjugated misfolded proteins, we performed an in vitro ubiquitination assay using a mixture of unmodified and SUMO2-modified Atxn1 82Q proteins (Figure 6D). In the presence of increasing doses of RNF4, the SUMO2-modified Atxn1 82Q proteins, which were of relatively low molecular weight (Figure 6E, lanes 1, 6, and 9), were progressively converted to higher-molecular-weight species that were also modified by ubiquitin (lanes 2–4, 7–9, and 12–14). In contrast, the unmodified Atxn1 82Q protein was not ubiquitinated (lanes 1–4). Therefore, RNF4 is a ubiquitin ligase for SUMO2/3-modified, but not unmodified, Atxn1 82Q protein.

RNF4 possesses both ubiquitin ligase and SUMO-binding activities (Sun et al., 2007). To ascertain the involvement of these activities in degrading Atxn1 82Q, we generated RNF4 mutants defective in either ubiquitin ligase (CS and CS1) or SUMO-binding (SIM^m) activity (Figure S6C). CS and CS1, albeit losing their ubiquitin E3 activity (Figure S6D), were still able to colocalize with Atxn1 82Q inclusions (Figure 6F). SIM^m, on the other hand, retained a substantial level of ubiquitin ligase activity (Figure S6E), but failed to colocalize with Atxn1 82Q inclusions

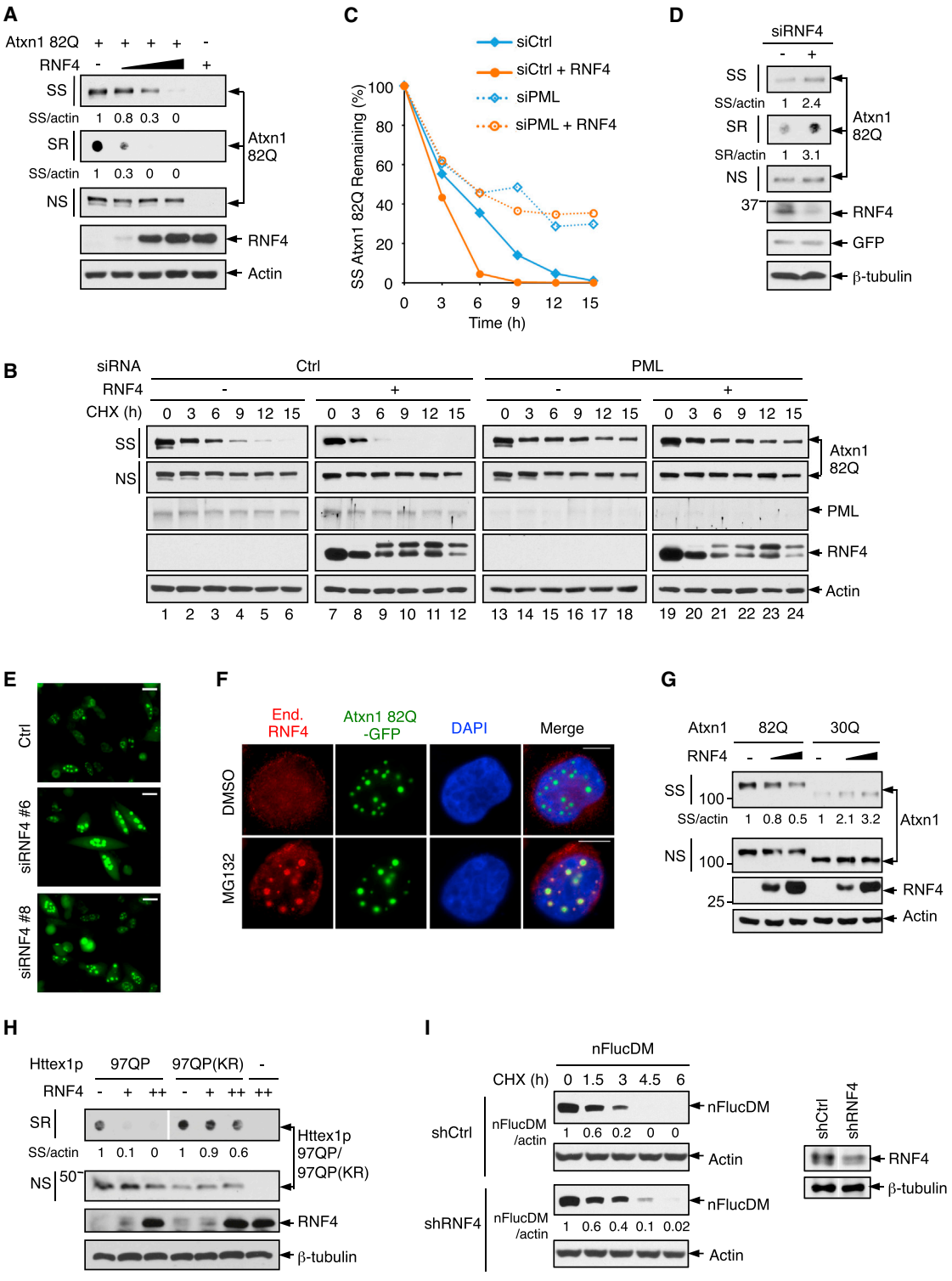

Figure 5. A Role of RNF4 in the Degradation of Atxn1 82Q

(A) Levels of Atxn1 82Q-GFP in HeLa cells without and with RNF4 overexpression.

(B and C) Effect of RNF4 overexpression on Atxn1 82Q-GFP stability in control and PML-depleted HeLa cells, analyzed by CHX treatment and WB. Relative SS Atxn1 82Q/actin ratios are shown in (C).

(D) Levels of FLAG-Atxn1 82Q in HeLa cells pretreated with a control siRNA (–) or a combination of three RNF4 siRNAs.

(E) Representative fluorescent images of Atxn1 82Q-GFP in control and RNF4-knockdown HeLa cells. Scale bar, 20 μm

(legend continued on next page)

(Figure 6G). Neither of the RNF4 mutant classes was capable of removing aggregated Atxn1 82Q (Figure 6H). Collectively, these results suggest that RNF4 binds to SUMO2/3-modified misfolded proteins via its SIM region and ubiquitinates these proteins via its ligase activity.

Although forced expression of PML led to effective clearance of aggregated Atxn1 82Q in control cells, this ability was greatly diminished in RNF4-depleted cells (Figure 6I). Reciprocally, forced expression of RNF4, albeit highly effective in accelerating Atxn1 82Q degradation in control cells, failed to do so in PML-depleted cells (Figure 5B, lanes 19–24 versus lanes 7–12; and Figure 5C). Moreover, in PML-depleted cells, which displayed high Atxn1 82Q levels, silencing RNF4 did not further elevate the levels of Atxn1 82Q (Figure S6F). These results indicate mutual dependence of PML and RNF4 in the degradation of Atxn1 82Q.

PML Deficiency Exacerbates Behavioral and Pathological Phenotypes in a Mouse Model of SCA1

The results described above revealed a PQC system that degrades Atxn1 82Q and likely other nuclear misfolded proteins through sequential PML-mediated SUMOylation and RNF4-mediated ubiquitination. To investigate the physiological role of this system, we used a mouse model of SCA1 (B05), which expresses the *Atxn1 82Q* transgene (*Atxn1*$^{tg/-}$) in the cerebellar Purkinje cells. Resembling human SCA1 patients, B05 mice develop ataxia and neurological abnormalities with increasing age (Burright et al., 1995). The loss of RNF4 in mice results in embryonic lethality (Hu et al., 2010), precluding the analysis of its effect on B05 mice. However, *PML*-knockout (*PML*$^{-/-}$) mice are viable and appear to develop normally (Wang et al., 1998). We crossbred B05 mice with *PML*$^{-/-}$ and *PML*-wild-type (*PML*$^{+/+}$) mice and compared the littermates of all genotypes—*PML*$^{+/+}$, *PML*$^{+/-}$, and *PML*$^{-/-}$, *PML*$^{+/+}$*:Atxn1*$^{tg/-}$, *PML*$^{+/-}$*:Atxn1*$^{tg/-}$, and *PML*$^{-/-}$*:Atxn1*$^{tg/-}$—for both motor performance and neuropathology.

Motor performance—including balance, coordination, and endurance—was evaluated using a Rotarod apparatus with accelerating speed. To determine whether any potential behavioral defects were due to a progressively diminished capacity, as opposed to a developmental impairment, we examined mice at different ages. To rule out the influence of the long-term motor memory, only naive animals were used, each being tested for 4 consecutive days.

At 7 weeks of age, all mice performed similarly on the Rotarod (Figure 7A). Although some differences were observed among mice of distinct genotypes, they were not statistically significant (ANOVA $p = 0.53$), suggesting that *PML*$^{-/-}$ mice did not have pre-existing impairments in their motor functions. At 11 weeks of age, all mice lacking the *Atxn1 82Q* transgene (*PML*$^{+/+}$, *PML*$^{+/-}$, and *PML*$^{-/-}$) still showed no statistical difference in their performance (ANOVA $p = 0.33$) (Figure 7B), and *PML*$^{+/+}$ and *PML*$^{+/+}$*:Atxn1*$^{tg/-}$ also performed similarly. These observations suggest that either *PML* deficiency or *Atxn1 82Q* transgene expression alone was insufficient to cause motor defects at this age. Interestingly, *PML*$^{-/-}$*:Atxn1*$^{tg/-}$ showed severe impairments in Rotarod performance compared to either *PML*$^{+/+}$*:Atxn1*$^{tg/-}$ or *PML*$^{-/-}$ mice. Although these three groups of animals were comparable at the beginning of the 4 consecutive testing days, unlike the other two groups, *PML*$^{-/-}$*:Atxn1*$^{tg/-}$ mice showed minimal improvement over time. The lack of improvement of *PML*$^{-/-}$*:Atxn1*$^{tg/-}$ mice on the Rotarod was reminiscent of *Atxn1*$^{tg/-}$ mice at advanced stages (Clark et al., 1997). The *PML* heterozygous counterparts (*PML*$^{+/-}$*:Atxn1*$^{tg/-}$ mice) displayed an intermediate impairment on the Rotarod (ANOVA $p = 0.0004$ for the three *Atxn1*$^{tg/-}$ groups) (Figure 7B). Thus, *PML* deficiency aggravates motor defects of the *Atxn1*$^{tg/-}$ mice.

The major neuropathological phenotype of the *Atxn1*$^{tg/-}$ mice is the degeneration of Purkinjie cells, a constituent of the top layer (the molecular layer) of the cerebellar cortex. This degeneration is manifested initially in the shrinkage of the molecular layer and the atrophy of Purkinje cell dendrites, and later in the loss of Purkinje cell bodies (Burright et al., 1995; Clark et al., 1997). At 12 weeks of age, *PML*$^{+/-}$ and *PML*$^{-/-}$ mice showed only a slight and statistically insignificant shrinkage in the molecular layers, while *PML*$^{+/+}$*:Atxn1*$^{tg/-}$ mice exhibited a discernible shrinkage, compared to *PML*$^{+/+}$ mice (Figures 7C and 7D). Because *PML*$^{+/+}$*:Atxn1*$^{tg/-}$ mice performed similarly on the Rotarod to *PML*$^{+/+}$ mice (Figure 7B), neurodegeneration in *PML*$^{+/+}$*:Atxn1*$^{tg/-}$ mice might not have reached a critical threshold. This nonlinear correlation between behavioral and pathological phenotypes of the SCA1 transgenic model has been previously observed (Gehrking et al., 2011). Importantly, compared to *PML*$^{+/+}$*:Atxn1*$^{tg/-}$ mice, *PML*$^{+/-}$*:Atxn1*$^{tg/-}$ and *PML*$^{-/-}$*:Atxn1*$^{tg/-}$ mice displayed a moderate and a strong further reduction, respectively, in the thickness of molecular layer (Figures 7C and 7D). This correlated with worsening performance of these animals on the Rotarod (Figure 7B). Thus, PML deficiency aggravates the shrinkage of the molecular layer in *Atxn1*$^{tg/-}$ mice.

We also examined dendritic arborization of Purkinje cells by immunofluorescence staining with an antibody against the Purkinje cell-specific protein calbindin. At 12 weeks of age, the fluorescence intensity of Purkinje cell dendrites in all groups containing the *Atxn1 82Q* transgene was reduced to very low levels that precluded precise comparison (Figures S7A and S7B). Of note, compared to *PML*$^{+/+}$ littermates, *PML*$^{-/-}$ mice already showed a strong reduction in dendritic arborization of Purkinje cells, while *PML*$^{+/-}$ mice showed an intermediate reduction (Figures S7A and S7B). These results indicate that PML itself has a role in protecting against neurodegeneration.

Despite the thinning of the molecular layer and the loss of Purkinje cell dendrites that were associated with *PML* deficiency, no significant difference in Purkinje cell population was

(F) Localization of Atxn1 82Q-GFP and endogenous RNF4 in HeLa cells treated with vehicle (DMSO) or MG132. Scale bar, 10 μm.
(G and H) Levels of FLAG-Atxn1 82Q and FLAG-Atxn1 30Q (G) or HA-Httex1p 97QP and HA-Httex1p 97QP(KR) (H) in HeLa cells without and with RNF4 overexpression.
(I) Stability of nFlucDM-GFP in HeLa cells stably expressing shCtrl and shRNF4 (left) and the levels of RNF4 in these cells (right).
See also Figure S5.

Please cite this article in press as: Guo et al., A Cellular System that Degrades Misfolded Proteins and Protects against Neurodegeneration, Molecular Cell (2014), http://dx.doi.org/10.1016/j.molcel.2014.04.030

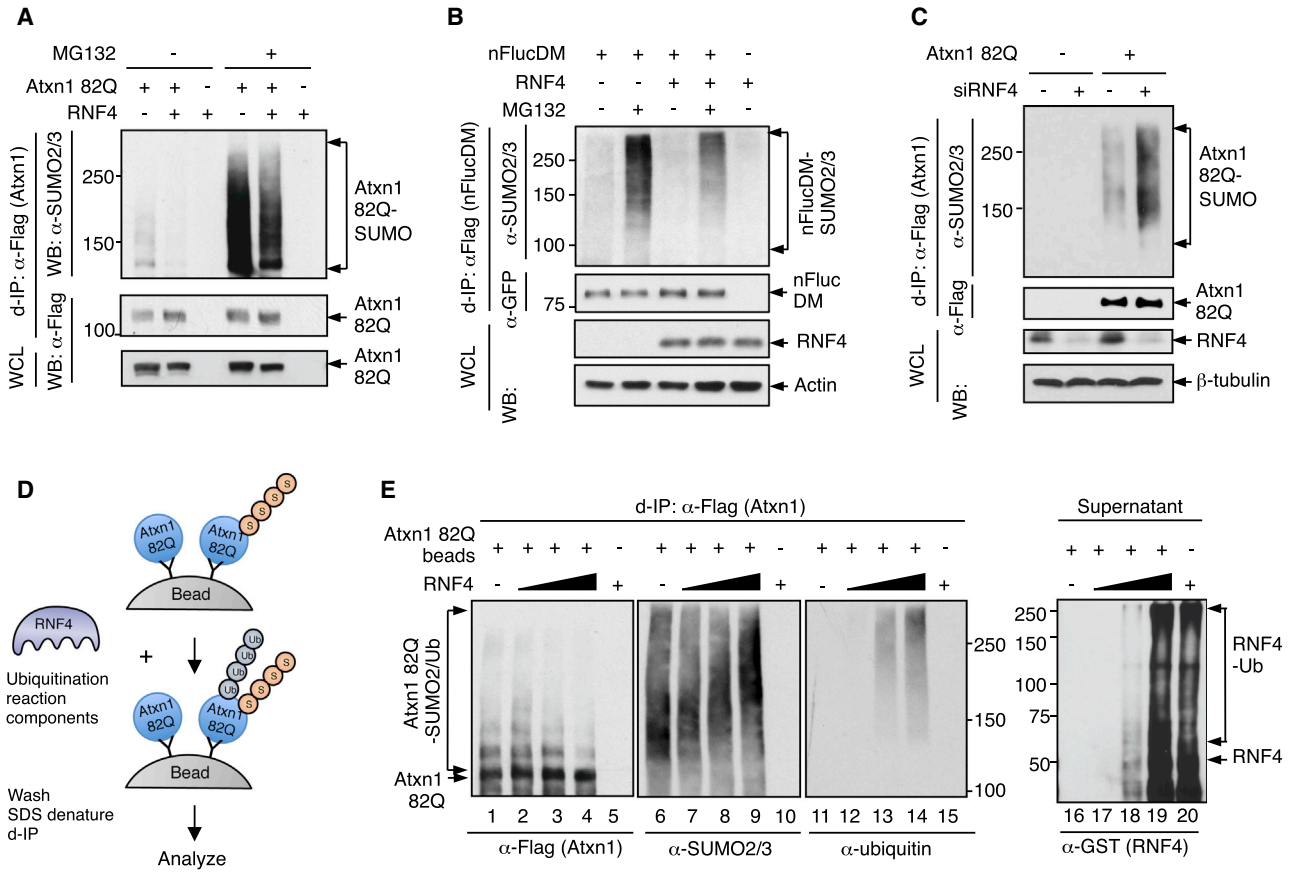

(legend on next page)

Please cite this article in press as: Guo et al., A Cellular System that Degrades Misfolded Proteins and Protects against Neurodegeneration, Molecular Cell (2014), http://dx.doi.org/10.1016/j.molcel.2014.04.030

observed among 12-week-old animals of different genotypes (Figure S7C). At 1 year of age, *PML*$^{-/-}$ mice displayed only a mild (11.0%) and statistically insignificant ($p = 0.107$) reduction in the number of Purkinje cells compared to *PML*$^{+/+}$ mice, while *PML*$^{+/+}$*:Atxn1*$^{tg/-}$ mice displayed a noticeable reduction (Figures 7E and 7F). Of note, *PML*$^{-/-}$*:Atxn1*$^{tg/-}$ mice showed a significant further reduction in Purkinje cell density compared to *PML*$^{+/+}$*:Atxn1*$^{tg/-}$ mice (~24%, $p = 0.0023$), and *PML*$^{+/-}$*:Atxn1*$^{tg/-}$ mice showed an intermediate cell loss (Figures 7E and 7F). Again, these results demonstrate that PML deficiency worsens the neuropathological defects caused by the *Atxn1 82Q* transgene.

Neurodegeneration of B05 mice is accompanied by the formation of ubiquitin-positive Atxn1 82Q inclusions in Purkinje cells (Clark et al., 1997). To determine the effect of PML on Atxn1 82Q nuclear inclusions, we quantified Purkinje cells with these inclusions in mice at 12 weeks of age. *PML* deficiency alone did not result in the formation of aggregates (Figure S7D), but it significantly increased the number of aggregate-containing Purkinje cells in Atxn1 82Q transgenic mice (Figures 7G and 7H). Collectively, these results suggest that endogenous PML plays a role in preventing accumulation of misfolded proteins in SCA1 animals and suppressing the progression of this neurodegenerative disease.

DISCUSSION

Here we present evidence for a PQC system that degrades misfolded proteins in mammalian cell nuclei. This system consists of a recognition branch, PML, which selectively binds to misfolded proteins and marks these proteins with poly-SUMO2/3 chains, and an effector branch, RNF4, which ubiquitinates SUMOylated misfolded proteins and targets them for proteasomal degradation. This relay system likely provides a critical link between misfolded proteins and the proteasome in mammalian cells, and it may play an important role in the protection against neurodegeneration and other proteopathies (Figure 7I).

Selective Recognition of Misfolded Proteins by PML

The exquisite selectivity of this system resides in PML, which contains at least two SRSs. SRS1, consisting of the CC region within the TRIM/RBCC motif, favors CC structures on pathogenic polyQ proteins and perhaps other misfolded proteins. SRS2, consisting of the C-terminal 63 amino acids, recognizes short peptides enriched in both aromatic (Phe, Trp, and Tyr) and positively charged (Arg and Lys) amino acids. SRS2 is similar to the bacterial Hsp100 ClpB (Schlieker et al., 2004), except that SRS2 also favors peptides containing Leu, a residue that is often exposed in misfolded proteins and is engaged by Hsp70 (Rüdiger et al., 1997). Thus, SRS2 displays a hybrid substrate specificity of ClpB and Hsp70. These observations indicate that PML can recognize structures or regions that are commonly found in misfolded proteins.

A Role for SUMOylation in Degrading Misfolded Proteins

Conjugation to SUMO is a major posttranslational modification, occurring on numerous proteins and vital to most eukaryotic life. Yet, beyond the generalization that it alters protein-protein interactions, the physiological function of SUMOylation remains elusive (Wilkinson and Henley, 2010). A prominent feature of the PML-RNF4 system is the involvement of SUMO2/3 modification prior to ubiquitination (Figures 3, 4, and S4). It was observed previously that conjugation of SUMO2/3 to cellular proteins is markedly enhanced by protein-denaturing stresses (Saitoh and Hinchey, 2000). The evidence presented in the current study provides an explanation for this observation, and suggests that a principal physiological function of SUMO2/3 modification is likely to facilitate the degradation of misfolded proteins, acting in concert with ubiquitination.

SUMO conjugation enhances protein solubility (Panavas et al., 2009). Because aggregated proteins cannot be effectively degraded by the proteasome (Verhoef et al., 2002), enhancing protein solubility may be a beneficial effect conferred by PML prior to ubiquitination. Moreover, the extent of SUMOylation may enable the "triage decision" as to whether a given misfolded protein is selected for refolding or degradation. Consistent with this notion, conjugation to a single SUMO appears to be sufficient to enhance protein solubility (Panavas et al., 2009), and thus may facilitate refolding. In contrast, conjugation to SUMO2/3 chains is needed for effective recognition by the four tandem SIMs on RNF4 for ubiquitination and degradation (Tatham et al., 2008). Such chains may form after unsuccessful refolding attempts.

SUMOylation of misfolded proteins has been reported to either promote or inhibit neurodegenerative diseases (Martin et al., 2007). These seemingly contradictory observations may be reconciled by the distinct functions of SUMO1 and SUMO2/3 in the removal of misfolded proteins (Figure 3), and by the dichotomy between the functions of SUMOylation: enhancing solubility of an abnormal protein (which may enhance its toxicity) and promoting its degradation. Thus, the outcome of elevated SUMOylation likely depends on whether it can be matched by the cellular degradative capacity.

A Potential Major PQC System

Proteins in the nucleus may harbor mutations or sustain acute and chronic damages, as proteins elsewhere do. The highly

Figure 6. RNF4 Promotes the Ubiquitination and Degradation of SUMO2/3-Modified Atxn1 82Q

(A and B) Levels of SUMOylated FLAG-Atxn1 82Q (A) and FLAG-nFlucDM-GFP (B), in the absence or presence of RNF4, in HeLa cells treated with or without MG132. d-IP products with similar levels of unmodified proteins, as well as WCL, were analyzed.

(C) Levels of SUMOylated FLAG-Atxn1 82Q in HeLa cells that were pretreated with a control siRNA or a combination of RNF4 siRNAs, analyzed as in (A).

(D and E) Unmodified and SUMO2-modified FLAG-Atxn1 82Q proteins conjugated on M2 beads (+), or control M2 beads (−), were incubated with ubiquitination reaction mixture, in the absence or presence of GST-RNF4. (D) A schematic diagram of the experimental design. (E) WB analysis of FLAG-Atxn1 82Q (left) and GST-RNF4 (right).

(F and G) Localization of Atxn1 82Q-GFP and RNF4 proteins (detected by anti-FLAG antibody) in HeLa. Scale bar, 10 μm.

(H) Effect of the indicated RNF4 proteins on Atxn1 82Q-GFP levels in HeLa cells.

(I) Effect of PML overexpression on Atxn1 82Q-GFP levels in HeLa cells that were pretreated with control or RNF4 siRNA.

See also Figure S6.

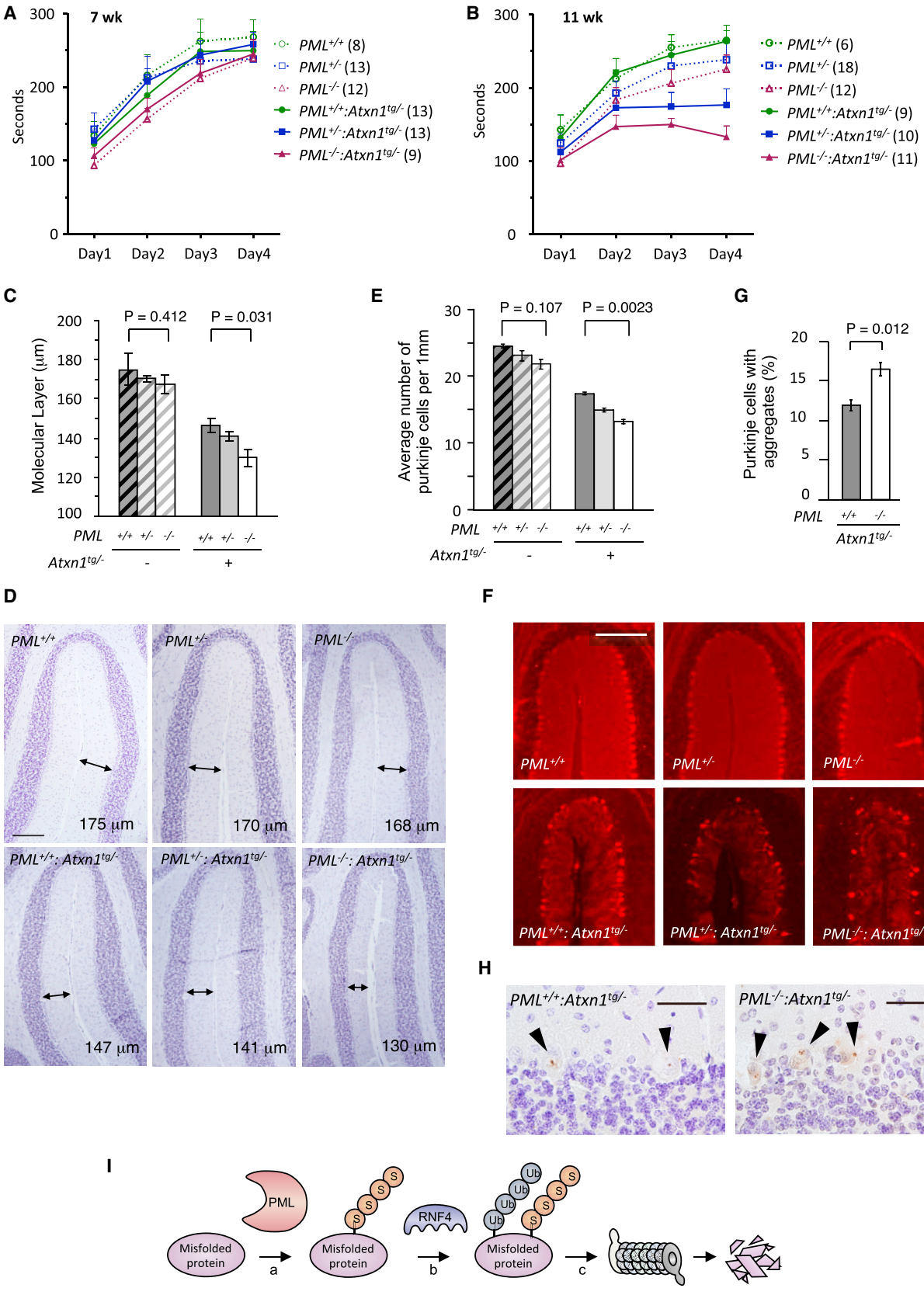

(legend on next page)

crowded environment of the nucleus likely makes it especially challenging to maintain protein quality. The ubiquitin-proteasome pathway is expected to be the main degradative system in the nucleus, where autophagy is not known to operate. Previous studies have implicated a few ubiquitin ligases, such as yeast San1 and Doa10 and mammalian UHRF-2 and E6-AP, in the degradation of nuclear misfolded proteins (Cummings et al., 1999; Deng and Hochstrasser, 2006; Gardner et al., 2005; Iwata et al., 2009). Nevertheless, the predominantly nuclear localization of PML, along with the potent effect of PML and RNF4 on diverse misfolded nuclear proteins, suggests that the PML-RNF4 system is likely a major PQC system in mammalian cell nuclei.

The TRIM family of proteins is shared among metazoans, from approximately 20 members in *C. elegans* to over 70 in mice and humans (Ozato et al., 2008). We previously demonstrated that at least several other TRIM proteins also possess SUMO E3 activity (Chu and Yang, 2011). Given their localization to the cytoplasm in addition to the nucleus (Ozato et al., 2008), we speculate that TRIM proteins also participate in PQC in the cytoplasm. The rapid expansion of the TRIM proteins during evolution might in part be a response to the increasing complexity of managing protein quality in cells of longer-living animals.

RNF4 is conserved among vertebrates (Sun et al., 2007). SUMO-dependent ubiquitin ligases are also present in low eukaryotic species (Sun et al., 2007), and are involved in the degradation of at least one mutant yeast transcription factor (Wang and Prelich, 2009). Thus, it is also possible that systems analogous to the PML-RNF4 system may play a role in maintaining protein quality in these organisms.

The PML-RNF4 System and Neurodegeneration

PML$^{-/-}$ mice have been extensively characterized for a variety of phenotypes including tumorigenesis (Wang et al., 1998). The present study indicates a role for PML in protection from neurodegeneration (Figures 7 and S7). Neurodegenerative disorders including SCAs and HD are usually late-onset diseases. Accumulating evidence suggests a progressive decline in PQC during aging (Balch et al., 2008). The strong effect of the PML-RNF4 on pathogenic proteins associated with SCA1, HD, and ALS and of PML deficiency on the progression of the SCA1 mouse model, along with the accumulation of PML in neuronal inclusions in patients with various neurodegenerative diseases (Skinner et al., 1997; Takahashi et al., 2003), suggests that insufficiency or dysfunction of the PML-RNF4 system may have a role in these diseases. We speculate that the PML-RNF4 system and analogous ones would be valuable targets in their treatment.

EXPERIMENTAL PROCEDURES

Cell Lysate Fractionation and Filter Retardation Assay

Cell lysates were made in NP-40-containing buffer and fractionated into supernatant (NS) and pellet by centrifugation. Both fractions were boiled in buffer containing 2% SDS and analyzed by western blot. A portion of the pellet was analyzed by a filter retardation assay for SR species.

Assays of Protein Half-Life

Cells were pulse labeled in Met- and Cys-free DMEM medium supplemented with [^{35}S]Met and [^{35}S]Cys, and then cultured in regular DMEM. Alternatively, cells were treated with CHX. Immunoprecipitated [^{35}S]Atxn1 82Q or unlabeled Atxn1 82Q in cell lysate was analyzed by autoradiography or western blot.

Screening of Cellulose-Bound Peptides for Binding to PML Domains

A peptide library (13-mers overlapping by ten amino acids) for firefly luciferase was prepared by automated spot synthesis (JPT Peptide Technologies). The peptide array membrane was probed with purified PML SRS1 and SRS2 fragments.

SUMOylation and Ubiquitination Analysis

Cells or in vitro reaction mixtures were boiled in buffer containing 2% SDS and then diluted in buffer without SDS or passed through a Bio-Spin chromatography column to reduce the SDS concentration. Proteins were immunoprecipitated (denaturing IP or d-IP) and analyzed by western blot.

Mouse Breeding and Behavioral Analysis

The heterozygous B05 transgenic mice *Atxn1*$^{tg/-}$ (on FVB background) (Burright et al., 1995) were mated with *PML*$^{-/-}$ (on 129Sv background) (Wang et al., 1998). *PML*$^{+/-}$*:Atxn1*$^{tg/-}$ mice from the F1 generation were mated with *PML*$^{-/-}$ or *PML*$^{+/+}$ to generate mice used for Rotarod tests and pathology. All animal experiments were performed in accordance with relevant guidelines and regulations and were approved by the University of Pennsylvania Institutional Animal Care and Use Committee (IACUC).

Immunostaining and Pathological Analysis of Mouse Cerebellum

Paraffin-embedded cerebellar midsagital sections were stained with indicated antibodies and visualized using a Leica SP5 II laser scanning confocal microscope, or stained with hematoxylin and visualized using an Olympus BX51 microscope.

Please see the Supplemental Information for the Supplemental Experimental Procedures and any associated references.

SUPPLEMENTAL INFORMATION

Supplemental Information includes seven figures and Supplemental Experimental Procedures and can be found with this article at http://dx.doi.org/10.1016/j.molcel.2014.04.030.

Figure 7. PML Deficiency Exacerbates Behavioral and Pathological Phenotypes of SCA1 Mouse Model

(A and B) Retention times (average + SEM) on accelerating Rotarod at 7 (A) and 11 (B) weeks of age, with the number of animals indicated in parenthesis.

(C and D) Cerebellar sections of 12-week-old animals were stained with hematoxylin. (C) Quantification of molecular layer thickness (means ± SEM, n = 3 mice/genotype). (D) Representative images of the staining. Scale bar, 200 μm.

(E and F) Cerebellar sections of 1-year-old animals were stained with an anti-calbindin antibody. (E) Quantitation of Purkinje cells, graphed as the average number of soma per 1 mm length (means ± SEM, n = 4 mice/genotype). (F) Representative images of the staining. Scale bar, 200 μm.

(G and H) Sections of the cerebellar cortex from 12-week-old mice were stained with an anti-ubiquitin antibody and counterstained with hematoxylin. (G) Percentage of Purkinje cells with aggregates (means ± SEM, n = 3 mice/genotype). (H) Representative images of the immunohistochemistry staining. Arrowheads indicate the ubiquitin positive aggregates in Purkinje cell bodies. Scale bar, 50 μm. No ubiquitin-positive aggregates were observed in Purkinje cells in mice without *Atxn1*$^{tg/-}$ (Figure S7D).

(I) A model for PQC by the PML-RNF4 system. PML recognizes misfolded proteins through SRSs and conjugates them with poly-SUMO2/3 chain through its SUMO E3 ligase activity (a). RNF4 ubiquitinates SUMOylated-misfolded proteins (b) and targets them for proteasomal degradation (c).

See also Figure S7.

ACKNOWLEDGMENTS

We thank H.T. Orr for providing B05 mice and P.P. Pandolfi for providing PML knockout mice. We thank Z. Yu, M.P. Heenan, S.J. Slattery, and E.F. Fischer for technical assistance; N.M. Bonini, M.S. Marks, Y. Argon, E.J. Brown, and V.M.-Y. Lee for advice; A. Stonestrom, T. Agrawal, K. Wang, X.-D. Fu, and C. O'Neill for help with manuscript preparation; and C.-X. Yuan and UPenn Abramson Cancer Center Proteomic Core for mass spectrometry analysis. We also thank the following scientists for the gifts of reagents: S.D. Barr, K.S. Chang, Y. Chen, M. Dasso, P. Goloubinoff, R.T. Hay, A.-M. Herr, S. Lindquist, J.L. Marsh, H.T. Orr, J.J. Palvimo, and S. Raychaudhuri. This work was supported, in part, by grants from NIH (CA088868 and GM060911); a grant from the Penn Medicine Neuroscience Center (PMNC); and a grant from the Penn Center for AIDS Research (CFAR), an NIH-funded program (P30 AI045008); to X.Y.

Received: September 4, 2013
Revised: January 31, 2014
Accepted: April 23, 2014
Published: May 29, 2014

REFERENCES

Balch, W.E., Morimoto, R.I., Dillin, A., and Kelly, J.W. (2008). Adapting proteostasis for disease intervention. Science *319*, 916–919.

Bernardi, R., and Pandolfi, P.P. (2007). Structure, dynamics and functions of promyelocytic leukaemia nuclear bodies. Nat. Rev. Mol. Cell Biol. *8*, 1006–1016.

Buchberger, A., Bukau, B., and Sommer, T. (2010). Protein quality control in the cytosol and the endoplasmic reticulum: brothers in arms. Mol. Cell *40*, 238–252.

Burright, E.N., Clark, H.B., Servadio, A., Matilla, T., Feddersen, R.M., Yunis, W.S., Duvick, L.A., Zoghbi, H.Y., and Orr, H.T. (1995). SCA1 transgenic mice: a model for neurodegeneration caused by an expanded CAG trinucleotide repeat. Cell *82*, 937–948.

Chen-Plotkin, A.S., Lee, V.M., and Trojanowski, J.Q. (2010). TAR DNA-binding protein 43 in neurodegenerative disease. Nat. Rev. Neurol. *6*, 211–220.

Chu, Y., and Yang, X. (2011). SUMO E3 ligase activity of TRIM proteins. Oncogene *30*, 1108–1116.

Clark, H.B., Burright, E.N., Yunis, W.S., Larson, S., Wilcox, C., Hartman, B., Matilla, A., Zoghbi, H.Y., and Orr, H.T. (1997). Purkinje cell expression of a mutant allele of SCA1 in transgenic mice leads to disparate effects on motor behaviors, followed by a progressive cerebellar dysfunction and histological alterations. J. Neurosci. *17*, 7385–7395.

Cummings, C.J., Reinstein, E., Sun, Y., Antalffy, B., Jiang, Y., Ciechanover, A., Orr, H.T., Beaudet, A.L., and Zoghbi, H.Y. (1999). Mutation of the E6-AP ubiquitin ligase reduces nuclear inclusion frequency while accelerating polyglutamine-induced pathology in SCA1 mice. Neuron *24*, 879–892.

Deng, M., and Hochstrasser, M. (2006). Spatially regulated ubiquitin ligation by an ER/nuclear membrane ligase. Nature *443*, 827–831.

Dobson, C.M. (2003). Protein folding and misfolding. Nature *426*, 884–890.

Fiumara, F., Fioriti, L., Kandel, E.R., and Hendrickson, W.A. (2010). Essential role of coiled coils for aggregation and activity of Q/N-rich prions and PolyQ proteins. Cell *143*, 1121–1135.

Gardner, R.G., Nelson, Z.W., and Gottschling, D.E. (2005). Degradation-mediated protein quality control in the nucleus. Cell *120*, 803–815.

Gehrking, K.M., Andresen, J.M., Duvick, L., Lough, J., Zoghbi, H.Y., and Orr, H.T. (2011). Partial loss of Tip60 slows mid-stage neurodegeneration in a spinocerebellar ataxia type 1 (SCA1) mouse model. Hum. Mol. Genet. *20*, 2204–2212.

Glover, J.R., and Lindquist, S. (1998). Hsp104, Hsp70, and Hsp40: a novel chaperone system that rescues previously aggregated proteins. Cell *94*, 73–82.

Goldberg, A.L. (2003). Protein degradation and protection against misfolded or damaged proteins. Nature *426*, 895–899.

Gupta, R., Kasturi, P., Bracher, A., Loew, C., Zheng, M., Villella, A., Garza, D., Hartl, F.U., and Raychaudhuri, S. (2011). Firefly luciferase mutants as sensors of proteome stress. Nat. Methods *8*, 879–884.

Hartl, F.U., Bracher, A., and Hayer-Hartl, M. (2011). Molecular chaperones in protein folding and proteostasis. Nature *475*, 324–332.

Hu, X.V., Rodrigues, T.M., Tao, H., Baker, R.K., Miraglia, L., Orth, A.P., Lyons, G.E., Schultz, P.G., and Wu, X. (2010). Identification of RING finger protein 4 (RNF4) as a modulator of DNA demethylation through a functional genomics screen. Proc. Natl. Acad. Sci. USA *107*, 15087–15092.

Iwata, A., Nagashima, Y., Matsumoto, L., Suzuki, T., Yamanaka, T., Date, H., Deoka, K., Nukina, N., and Tsuji, S. (2009). Intranuclear degradation of polyglutamine aggregates by the ubiquitin-proteasome system. J. Biol. Chem. *284*, 9796–9803.

Janer, A., Martin, E., Muriel, M.P., Latouche, M., Fujigasaki, H., Ruberg, M., Brice, A., Trottier, Y., and Sittler, A. (2006). PML clastosomes prevent nuclear accumulation of mutant ataxin-7 and other polyglutamine proteins. J. Cell Biol. *174*, 65–76.

Martin, S., Wilkinson, K.A., Nishimune, A., and Henley, J.M. (2007). Emerging extranuclear roles of protein SUMOylation in neuronal function and dysfunction. Nat. Rev. Neurosci. *8*, 948–959.

Nisole, S., Maroui, M.A., Mascle, X.H., Aubry, M., and Chelbi-Alix, M.K. (2013). Differential Roles of PML Isoforms. Front. Oncol. *3*, 125.

Orr, H.T., and Zoghbi, H.Y. (2007). Trinucleotide repeat disorders. Annu. Rev. Neurosci. *30*, 575–621.

Ozato, K., Shin, D.M., Chang, T.H., and Morse, H.C., 3rd. (2008). TRIM family proteins and their emerging roles in innate immunity. Nat. Rev. Immunol. *8*, 849–860.

Panavas, T., Sanders, C., and Butt, T.R. (2009). SUMO fusion technology for enhanced protein production in prokaryotic and eukaryotic expression systems. Methods Mol. Biol. *497*, 303–317.

Riley, B.E., Zoghbi, H.Y., and Orr, H.T. (2005). SUMOylation of the polyglutamine repeat protein, ataxin-1, is dependent on a functional nuclear localization signal. J. Biol. Chem. *280*, 21942–21948.

Rüdiger, S., Germeroth, L., Schneider-Mergener, J., and Bukau, B. (1997). Substrate specificity of the DnaK chaperone determined by screening cellulose-bound peptide libraries. EMBO J. *16*, 1501–1507.

Saitoh, H., and Hinchey, J. (2000). Functional heterogeneity of small ubiquitin-related protein modifiers SUMO-1 versus SUMO-2/3. J. Biol. Chem. *275*, 6252–6258.

Schlieker, C., Weibezahn, J., Patzelt, H., Tessarz, P., Strub, C., Zeth, K., Erbse, A., Schneider-Mergener, J., Chin, J.W., Schultz, P.G., et al. (2004). Substrate recognition by the AAA+ chaperone ClpB. Nat. Struct. Mol. Biol. *11*, 607–615.

Selkoe, D.J. (2003). Folding proteins in fatal ways. Nature *426*, 900–904.

Skinner, P.J., Koshy, B.T., Cummings, C.J., Klement, I.A., Helin, K., Servadio, A., Zoghbi, H.Y., and Orr, H.T. (1997). Ataxin-1 with an expanded glutamine tract alters nuclear matrix-associated structures. Nature *389*, 971–974.

Steffan, J.S., Agrawal, N., Pallos, J., Rockabrand, E., Trotman, L.C., Slepko, N., Illes, K., Lukacsovich, T., Zhu, Y.Z., Cattaneo, E., et al. (2004). SUMO modification of Huntingtin and Huntington's disease pathology. Science *304*, 100–104.

Sun, H., Leverson, J.D., and Hunter, T. (2007). Conserved function of RNF4 family proteins in eukaryotes: targeting a ubiquitin ligase to SUMOylated proteins. EMBO J. *26*, 4102–4112.

Takahashi, J., Fujigasaki, H., Iwabuchi, K., Bruni, A.C., Uchihara, T., El Hachimi, K.H., Stevanin, G., Dürr, A., Lebre, A.S., Trottier, Y., et al. (2003). PML nuclear bodies and neuronal intranuclear inclusion in polyglutamine diseases. Neurobiol. Dis. *13*, 230–237.

Tatham, M.H., Geoffroy, M.C., Shen, L., Plechanovova, A., Hattersley, N., Jaffray, E.G., Palvimo, J.J., and Hay, R.T. (2008). RNF4 is a poly-SUMO-specific E3 ubiquitin ligase required for arsenic-induced PML degradation. Nat. Cell Biol. *10*, 538–546.

Taylor, J.P., Hardy, J., and Fischbeck, K.H. (2002). Toxic proteins in neurodegenerative disease. Science *296*, 1991–1995.

Tyedmers, J., Mogk, A., and Bukau, B. (2010). Cellular strategies for controlling protein aggregation. Nat. Rev. Mol. Cell Biol. *11*, 777–788.

Verhoef, L.G., Lindsten, K., Masucci, M.G., and Dantuma, N.P. (2002). Aggregate formation inhibits proteasomal degradation of polyglutamine proteins. Hum. Mol. Genet. *11*, 2689–2700.

Wang, Z., and Prelich, G. (2009). Quality control of a transcriptional regulator by SUMO-targeted degradation. Mol. Cell. Biol. *29*, 1694–1706.

Wang, Z.G., Delva, L., Gaboli, M., Rivi, R., Giorgio, M., Cordon-Cardo, C., Grosveld, F., and Pandolfi, P.P. (1998). Role of PML in cell growth and the retinoic acid pathway. Science *279*, 1547–1551.

Wilkinson, K.A., and Henley, J.M. (2010). Mechanisms, regulation and consequences of protein SUMOylation. Biochem. J. *428*, 133–145.

Molecular Cell, Volume *55*

Supplemental Information

A Cellular System that Degrades Misfolded Proteins through Sequential SUMOylation and Ubiquitination

Lili Guo, Benoit I. Giasson, Alex Glavis-Bloom, Michael D. Brewer, James Shorter, Aaron D. Gitler, and Xiaolu Yang

Supplemental Information

A cellular system that degrades misfolded proteins through sequential SUMOylation and ubiquitination

Lili Guo, Benoit I. Giasson, Alex Glavis-Bloom, Michael D. Brewer, James Shorter, Aaron D. Gitler, and Xiaolu Yang

This file includes:

Supplemental Figure S1, related to Figure 1

Supplemental Figures S2 and S3, related to Figure 2

Supplemental Figure S4, related to Figures 3, 4

Supplemental Figure S5, related to Figure 5

Supplemental Figure S6, related to Figure 6

Supplemental Figure S7, related to Figure 7

Supplemental Figure Legends

Supplemental Experimental Procedures

Supplemental References

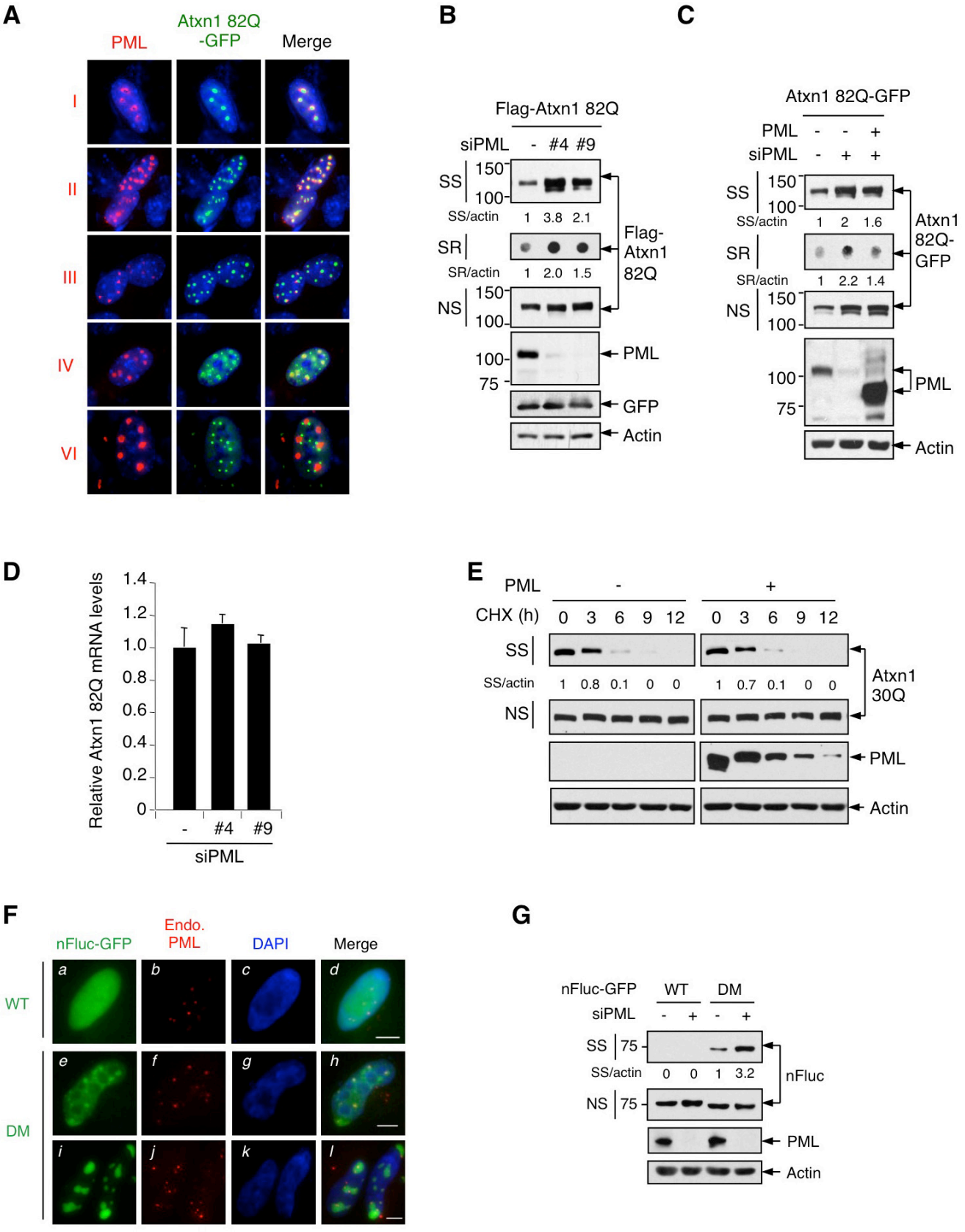
A
PML
Atxn1 82Q -GFP
Merge
I
II
III
IV
VI
B
Flag-Atxn1 82Q
siPML - #4 #9
SS
150
100
SS/actin 1 3.8 2.1
SR
SR/actin 1 2.0 1.5
NS
150
100
Flag-Atxn1 82Q
100
75
PML
GFP
Actin
C
Atxn1 82Q-GFP
PML - - +
siPML - + +
SS
150
100
SS/actin 1 2 1.6
SR
SR/actin 1 2.2 1.4
NS
150
100
Atxn1 82Q-GFP
100
75
PML
Actin
D
Relative Atxn1 82Q mRNA levels
1.4
1.2
1.0
0.8
0.6
0.4
0.2
0
- #4 #9
siPML
E
PML - +
CHX (h) 0 3 6 9 12 0 3 6 9 12
SS
SS/actin 1 0.8 0.1 0 0 1 0.7 0.1 0 0
NS
Atxn1 30Q
PML
Actin
F
nFluc-GFP
Endo. PML
DAPI
Merge
WT
DM
a
b
c
d
e
f
g
h
i
j
k
l
G
nFluc-GFP WT DM
siPML - + - +
SS 75
SS/actin 0 0 1 3.2
NS 75
nFluc
PML
Actin

Figure S2

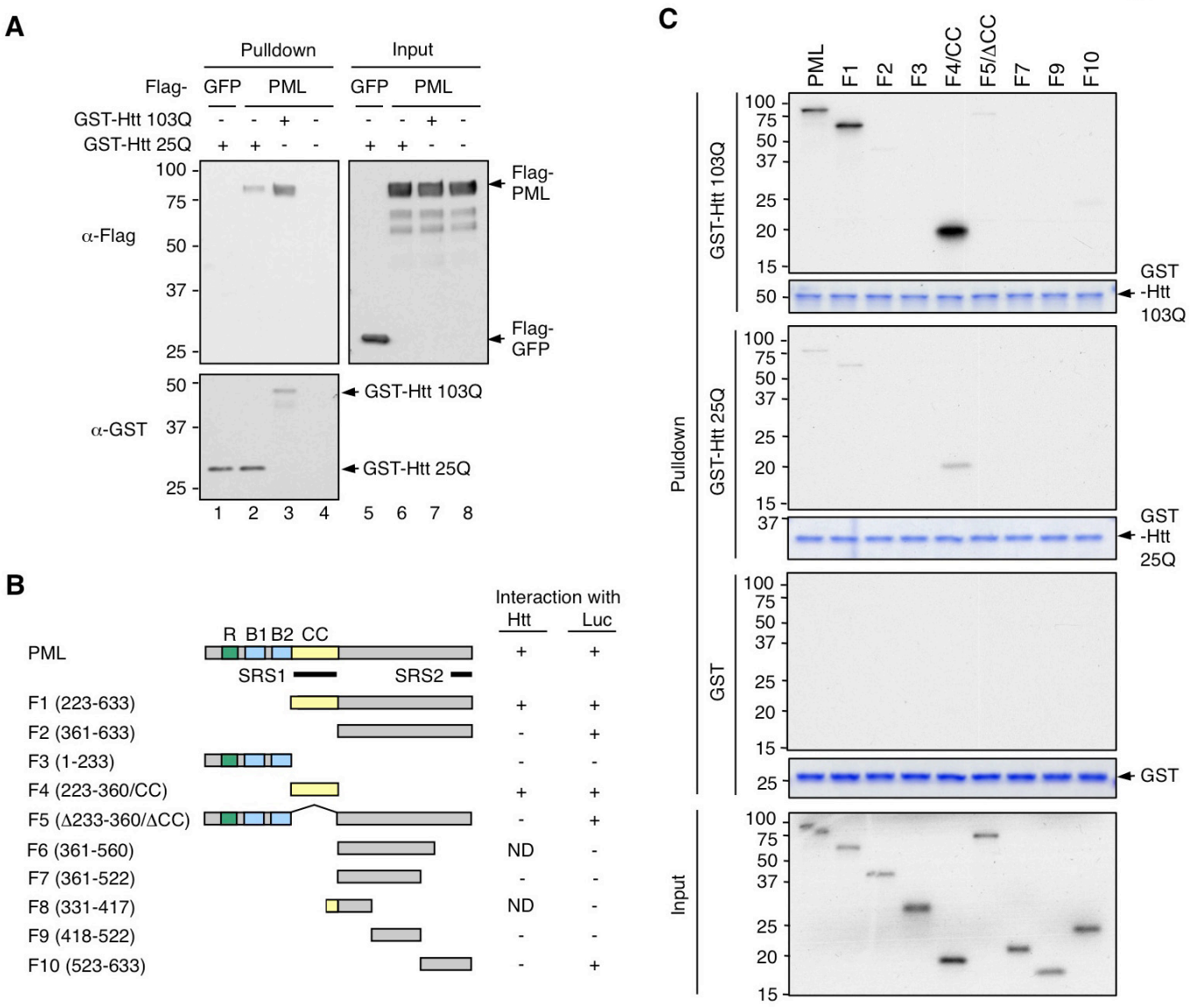
A
Pulldown
Input
Flag-
GFP
PML
GST-Htt 103Q
GST-Htt 25Q
α-Flag
α-GST
Flag-PML
Flag-GFP
GST-Htt 103Q
GST-Htt 25Q
B
Interaction with
Htt
Luc
R B1 B2 CC
SRS1
SRS2
PML
F1 (223-633)
F2 (361-633)
F3 (1-233)
F4 (223-360/CC)
F5 (Δ233-360/ΔCC)
F6 (361-560)
F7 (361-522)
F8 (331-417)
F9 (418-522)
F10 (523-633)
ND
C
PML
F1
F2
F3
F4/CC
F5/ΔCC
F7
F9
F10
Pulldown
GST-Htt 103Q
GST-Htt 25Q
GST
Input
GST-Htt 103Q
GST-Htt 25Q
GST
D
Htt 52Q MATLEKLMKAFESLKSFQQQQQQQQQQQQQQQQQQQQQQQQQQQQQQQQQQQQQQQQ
Htt 52Q cc-
E
N
M1
K31
V61
P91
S121
I151
F181
P211
V241
E271
I301
F331
A361
C391
G421
P451
P481
K531
PML
F4/CC

Figure S3

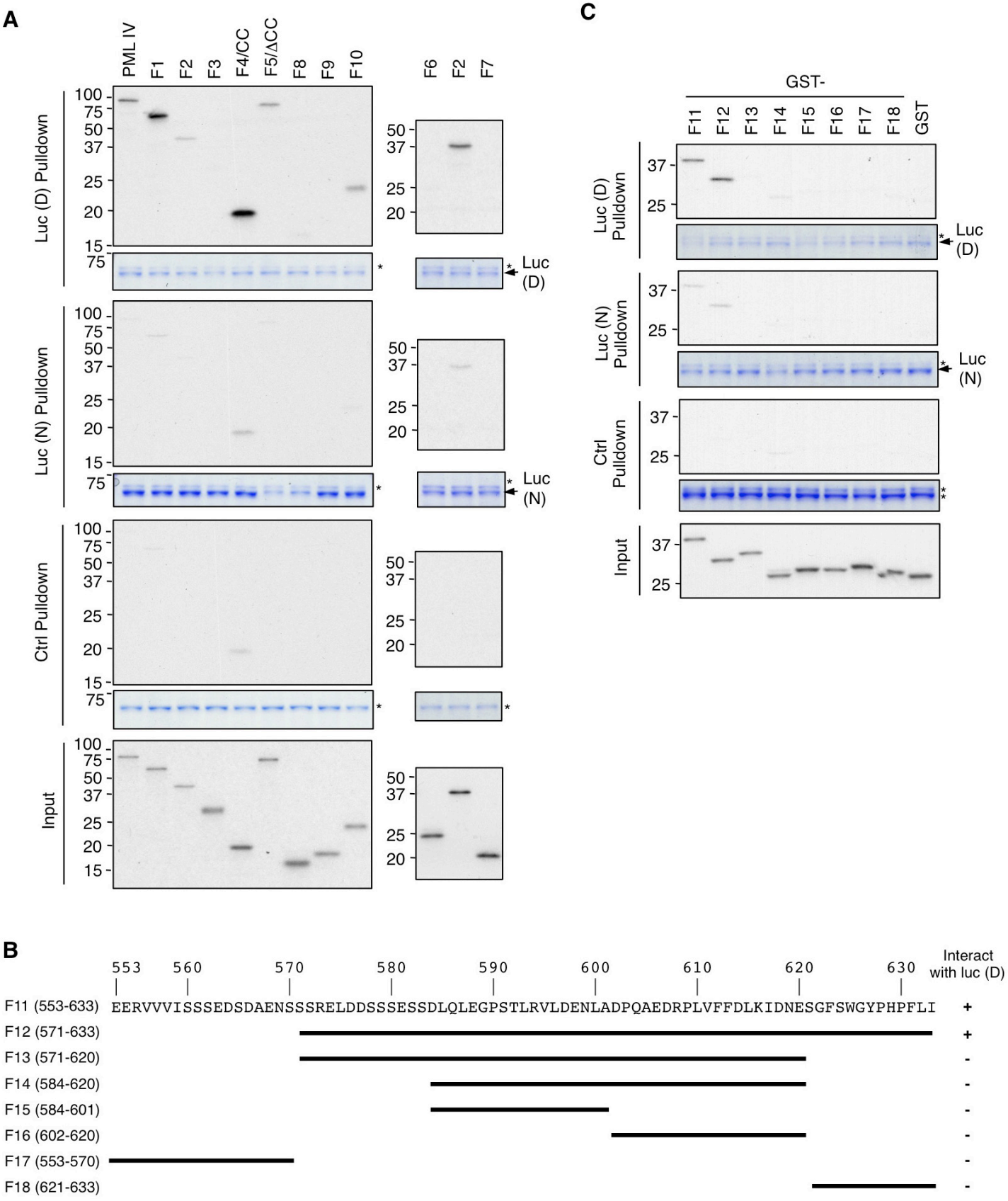
A
PML IV
F1
F2
F3
F4/CC
F5/ΔCC
F8
F9
F10
F6
F2
F7
Luc (D) Pulldown
Luc (N) Pulldown
Ctrl Pulldown
Input
Luc (D)
Luc (N)
C
GST-
F11
F12
F13
F14
F15
F16
F17
F18
GST
Luc (D) Pulldown
Luc (N) Pulldown
Ctrl Pulldown
Input
Luc (D)
Luc (N)
B
Interact with luc (D)
F11 (553-633) EERVVVISSSEDSDAENSSSRELDDSSSESSDLQLEGPSTLRVLDENLADPQAEDRPLVFFDLKIDNESGFSWGYPHPFLI +
F12 (571-633) +
F13 (571-620) -
F14 (584-620) -
F15 (584-601) -
F16 (602-620) -
F17 (553-570) -
F18 (621-633) -

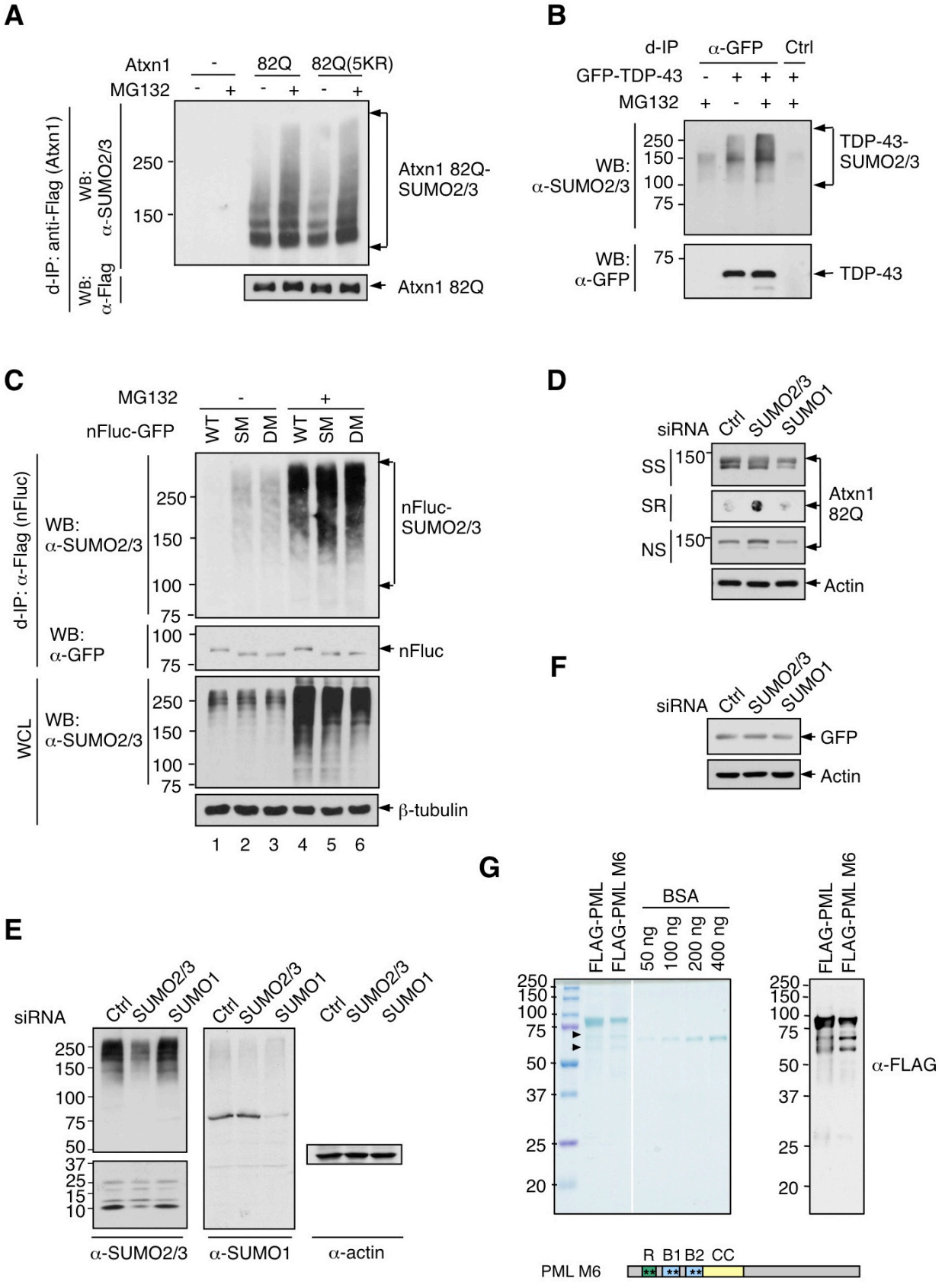
A
Atxn1
-
82Q
82Q(5KR)
MG132
- + - + - +
d-IP: anti-Flag (Atxn1)
WB: α-SUMO2/3
WB: α-Flag
250
150
Atxn1 82Q-SUMO2/3
Atxn1 82Q
B
d-IP
α-GFP
Ctrl
GFP-TDP-43
- + + +
MG132
+ - + +
WB: α-SUMO2/3
250
150
100
75
TDP-43-SUMO2/3
WB: α-GFP
75
TDP-43
C
MG132
-
+
nFluc-GFP
WT SM DM WT SM DM
d-IP: α-Flag (nFluc)
WB: α-SUMO2/3
250
150
100
75
nFluc-SUMO2/3
WB: α-GFP
100
75
nFluc
WCL
WB: α-SUMO2/3
250
150
100
75
β-tubulin
1 2 3 4 5 6
D
siRNA
Ctrl
SUMO2/3
SUMO1
SS
SR
NS
150
Atxn1 82Q
Actin
F
siRNA
Ctrl
SUMO2/3
SUMO1
GFP
Actin
E
siRNA
Ctrl
SUMO2/3
SUMO1
250
150
100
75
50
37
25
15
10
α-SUMO2/3
α-SUMO1
α-actin
G
FLAG-PML
FLAG-PML M6
BSA
50 ng
100 ng
200 ng
400 ng
250
150
100
75
50
37
25
20
α-FLAG
PML M6
R B1 B2 CC

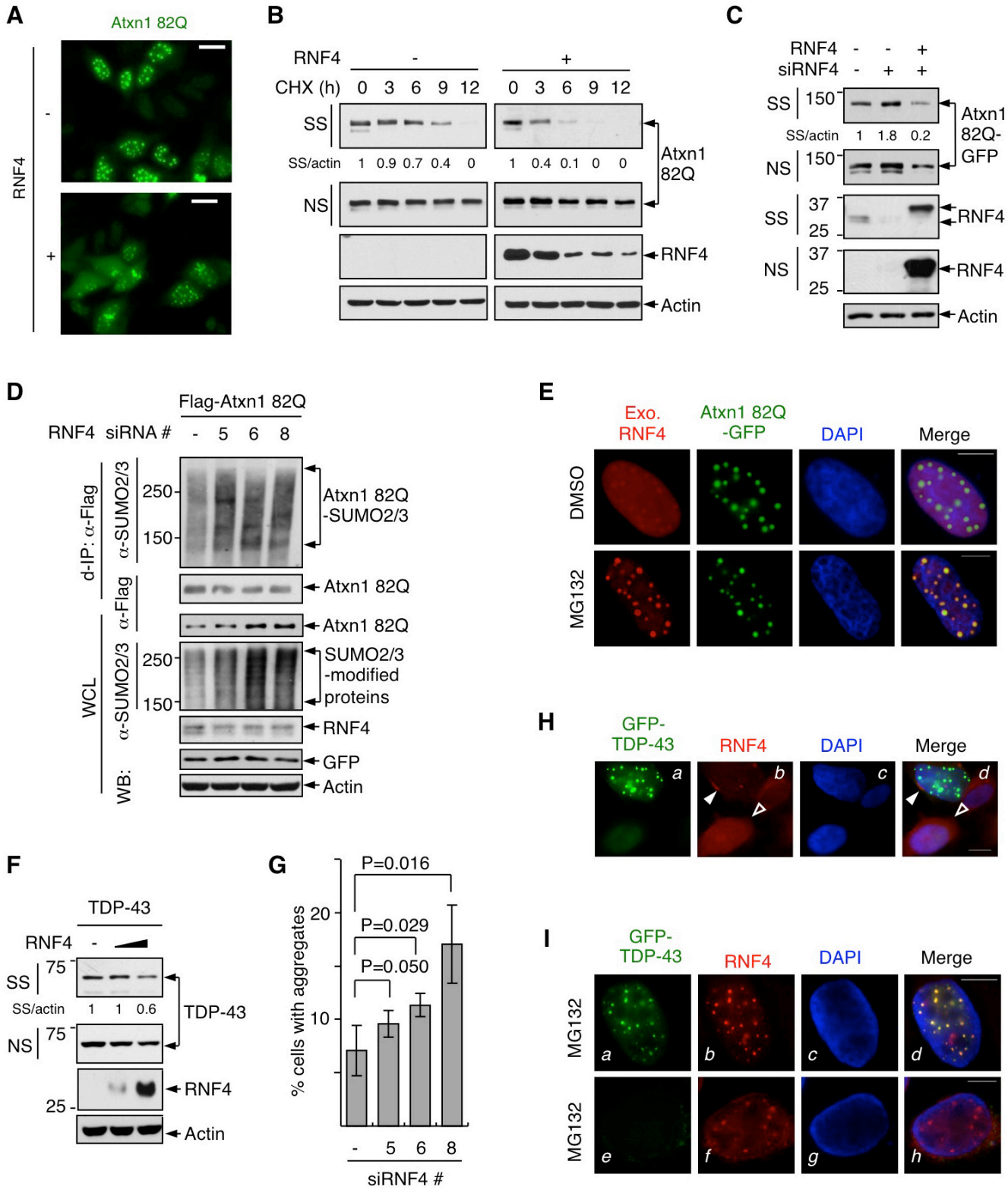
A
Atxn1 82Q
RNF4
-
+
B
RNF4
-
+
CHX (h) 0 3 6 9 12 0 3 6 9 12
SS
SS/actin 1 0.9 0.7 0.4 0 1 0.4 0.1 0 0
Atxn1 82Q
NS
RNF4
Actin
C
RNF4 - - +
siRNF4 - + +
SS 150
SS/actin 1 1.8 0.2
Atxn1 82Q-GFP
NS 150
SS 37 25
RNF4
NS 37 25
RNF4
Actin
D
Flag-Atxn1 82Q
RNF4 siRNA # - 5 6 8
d-IP: α-Flag
α-SUMO2/3
250
150
Atxn1 82Q -SUMO2/3
α-Flag
Atxn1 82Q
Atxn1 82Q
WCL
α-SUMO2/3
250
150
SUMO2/3 -modified proteins
RNF4
WB:
GFP
Actin
E
Exo. RNF4
Atxn1 82Q -GFP
DAPI
Merge
DMSO
MG132
F
TDP-43
RNF4 -
SS 75
SS/actin 1 1 0.6
TDP-43
NS 75
RNF4
25
Actin
G
P=0.016
P=0.029
P=0.050
20
10
% cells with aggregates
- 5 6 8
siRNF4 #
H
GFP-TDP-43
RNF4
DAPI
Merge
a
b
c
d
I
GFP-TDP-43
RNF4
DAPI
Merge
MG132
MG132
a
b
c
d
e
f
g
h

Figure S6

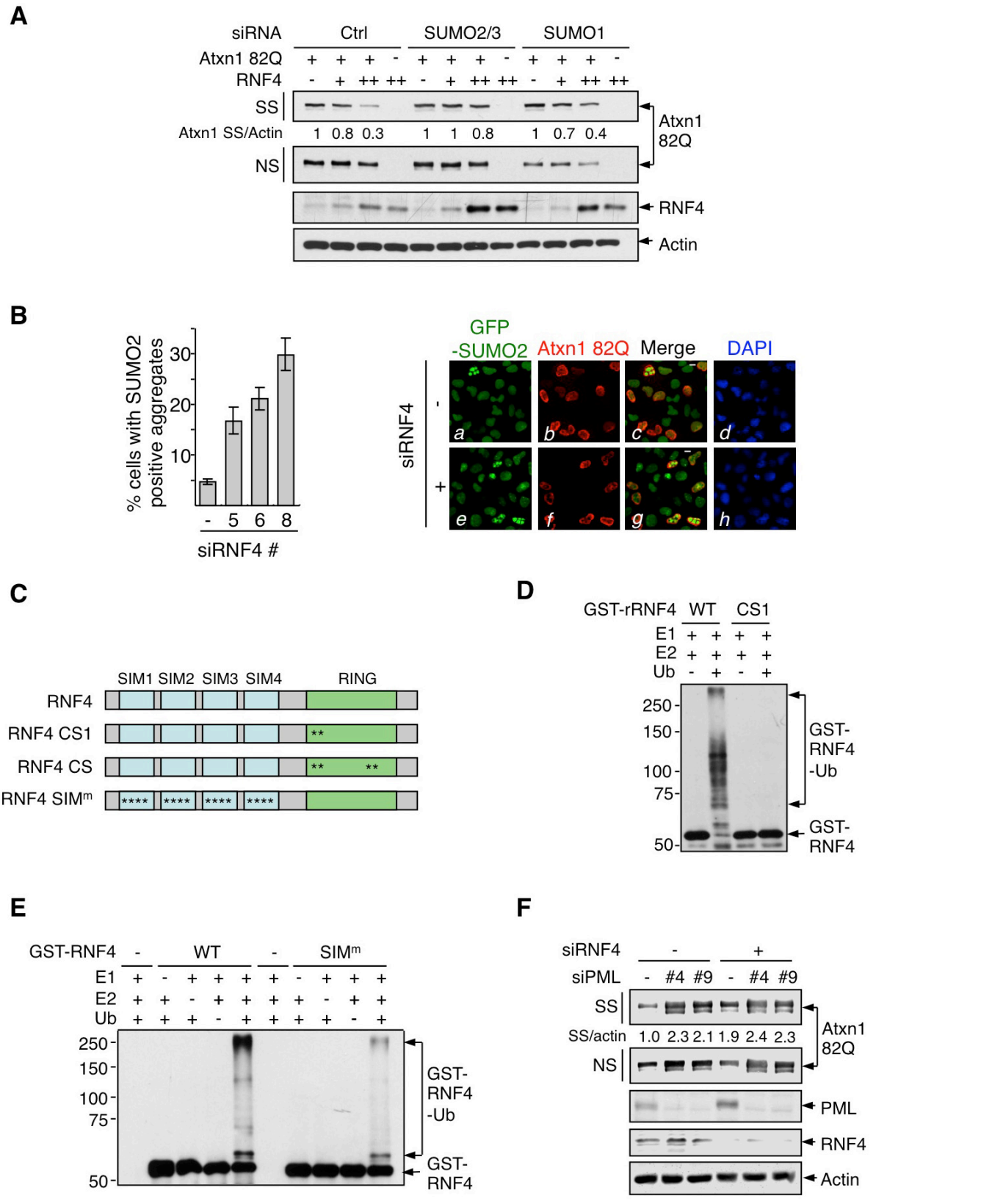
A
siRNA
Ctrl
SUMO2/3
SUMO1
Atxn1 82Q
RNF4
SS
Atxn1 SS/Actin
1 0.8 0.3 1 1 0.8 1 0.7 0.4
NS
Atxn1 82Q
RNF4
Actin
B
% cells with SUMO2 positive aggregates
30
20
10
- 5 6 8
siRNF4 #
GFP -SUMO2
Atxn1 82Q
Merge
DAPI
siRNF4
a b c d e f g h
C
SIM1 SIM2 SIM3 SIM4
RING
RNF4
RNF4 CS1
RNF4 CS
RNF4 SIMm
D
GST-rRNF4 WT CS1
E1
E2
Ub
250
150
100
75
50
GST-RNF4 -Ub
GST-RNF4
E
GST-RNF4
WT
SIMm
E1
E2
Ub
250
150
100
75
50
GST-RNF4 -Ub
GST-RNF4
F
siRNF4
siPML
#4 #9
SS
SS/actin
1.0 2.3 2.1 1.9 2.4 2.3
NS
Atxn1 82Q
PML
RNF4
Actin

Figure S7

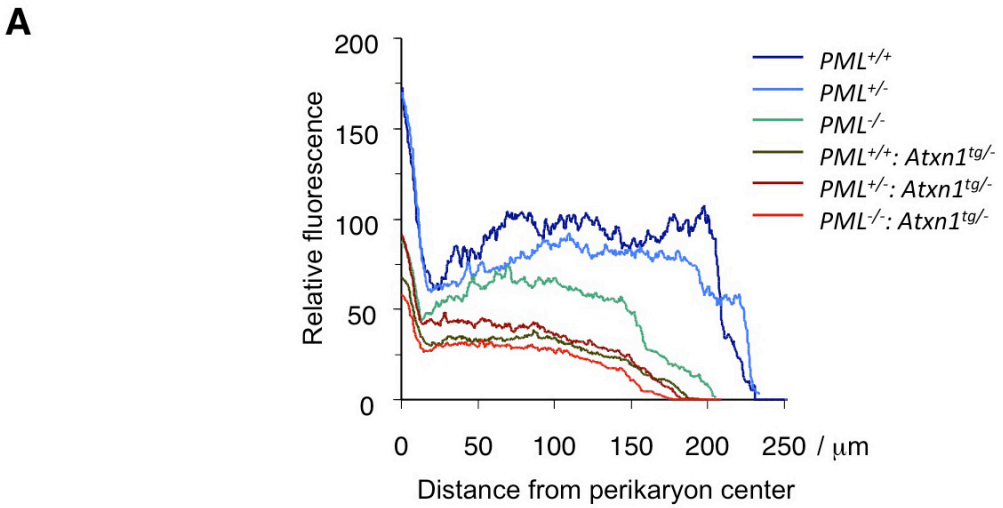
A
200
150
100
50
0
Relative fluorescence
0
50
100
150
200
250 / μm
Distance from perikaryon center
PML+/+
PML+/-
PML-/-
PML+/+: Atxn1tg/-
PML+/-: Atxn1tg/-
PML-/-: Atxn1tg/-

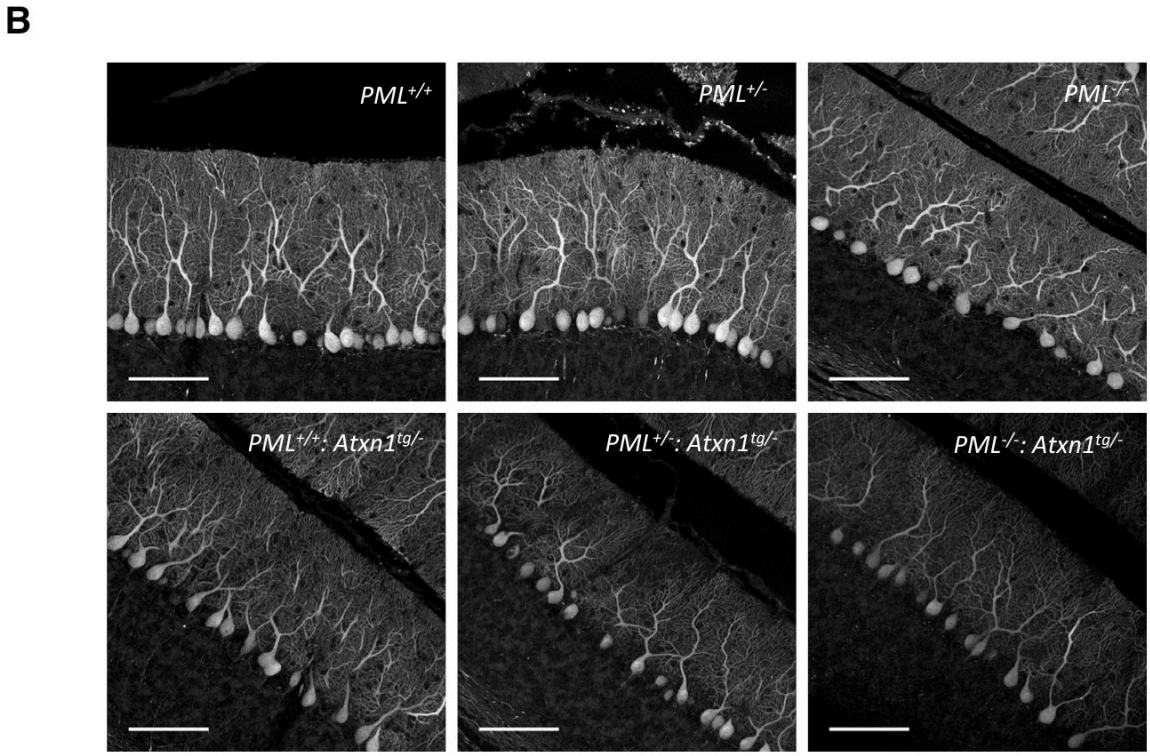
B
PML+/+
PML+/-
PML-/-
PML+/+: Atxn1tg/-
PML+/-: Atxn1tg/-
PML-/-: Atxn1tg/-

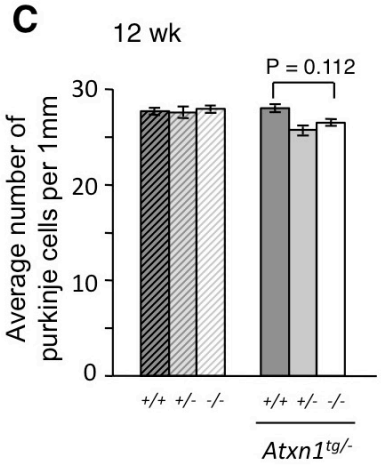
C
12 wk
P = 0.112
Average number of purkinje cells per 1mm
30
20
10
0
+/+ +/- -/-
+/+ +/- -/-
Atxn1tg/-

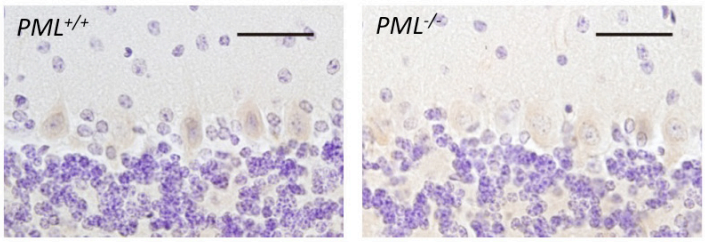
D
PML+/+
PML-/-

SUPPLEMENTAL FIGURE LEGENDS

Figure S1. PML co-localizes with Atxn1 82Q aggregates and decreases insoluble Atxn1 82Q (related to Figure 1).

(**A**) Atxn1 82Q-GFP was expressed in PML-deficient (*PML*$^{-/-}$) mouse embryonic fibroblasts (MEFs) together with each of the indicated PML isoforms. Cells were stained with anti-PML antibody (red) and DAPI (blue).

(**B**) Levels of FLAG-Atxn1 82Q in HeLa cells treated with a control siRNA (-), PML siRNA #4, or PML siRNA #9. Cell lysates were analyzed by Western blot and filter retardation assays. The ratios of Atxn1 82Q in the SS fraction versus actin, normalized to the control, are shown.

(**C**) HeLa cells were transfected with a control siRNA, PML siRNA #4 (which targeted the 5'UTR of the PML mRNA), or PML siRNA #4 plus a plasmid expressing the open reading frame of PML (hence resistant to the siRNA). Levels of Atxn1 82Q-GFP in various fractions were analyzed.

(**D**) HeLa cells were treated with control siRNA, PML siRNA #4, and PML siRNA #9 and then transfected with FLAG-Atxn1 82Q. The levels of the FLAG-Atxn1 82Q transcript were determined by quantitative RT-PCR normalized to levels of 18S rRNA.

(**E**) Atxn1 30Q-GFP was expressed in HeLa cells in the absence or presence of PML. Cells were then treated with CHX for the indicated times.

(**F**) HeLa cells were transfected with nFlucDM-GFP and the corresponding wild-type luciferase (WT) protein. Endogenous PML was detected by an anti-PML antibody (red), and DNA by DAPI (blue). Scale bar: 10 μm.

(**G**) PML knockdown leads to accumulation of insoluble mutant luciferase. HeLa cells were transfected with control or PML siRNA and then with nFluc-GFP or nFlucDM-GFP. The SR fraction contained very small amounts of nFlucDM-GFP (not shown).

Figure S2. Interaction of PML with pathogenic Htt proteins (related to Figure 2).

(**A**) PML preferentially interact with pathogenic Htt. Lysates of 293T cells expressing FLAG-GFP or FLAG-PML were incubated with GST-Htt 25Q or GST-Htt 103Q immobilized on glutathione beads (lanes 1-3 and 5-7), or with control glutathione beads (lanes 4 and 8). The input and pull-down fractions were analyzed by Western blot.

(**B**) Schematic representation of wild-type PML isoforms IV (aa 1-633) (called PML in the present work) and various deletion fragments (F1-F10). The RING domain (R), B1 box, B2 box, and coiled-coil region (CC) are labeled. Substrate recognition sites SRS1 and SRS2 are indicated by lines. The interaction of PML with pathogenic Htt proteins (Htt 103Q or 52Q) and denatured luciferase are shown. ND: not done.

(**C**) Interactions of full-length PML and PML deletion mutants with Htt. PML proteins were generated by coupled *in vitro* transcription/translation in the presence of [^{35}S]Met, and were incubated with purified GST-Htt 103Q, GST-Htt 25Q, or GST immobilized on glutathione beads. [^{35}S]Met-labeled proteins in the input and pull-down samples were analyzed by autoradiography, and GST proteins in the pull-down samples were analyzed by Coomassie staining. The three pull-down sample sets were analyzed at the same time and in the same way, including the amount of samples and the exposure duration of autoradiography. The input samples were exposed for a shorter period of time.

(**D**) Sequences of Htt 52Q and the CC-destabilizing (cc-) mutant. The amino acids in Htt 52Q that are changed to Pro in Htt 52Q cc- are shown in red.

(**E**) Interaction of purified PML CC region (shown on the right) with cellulose-bound luciferase peptide scans was assayed as in Figure 2D. * TEV protease (see Experimental Procedure).

Figure S3. Interaction of PML with denatured luciferase (related to Figure 2).

(**A**) Interaction of PML fragments with denatured luciferase. In vitro-translated, [^{35}S]-labeled full-length FLAG-PML and FLAG-PML deletion mutants were incubated with native or denatured luciferase immobilized on beads, or control beads. The input and beads-bound PML proteins were analyzed by autoradiography, and luciferase by Coomassie blue staining. *, Non-specific bands. The three pull down sample sets were analyzed at the same time and in the same way, including the amount of samples and the exposure duration of autoradiography. The input samples were exposed for a shorter period of time.

(**B** and **C**) Identification of the second substrate recognition site (SRS2) on PML. (B) PML deletion mutations encompassing amino acids at the C-terminus and summary of their interaction with denatured luciferase. (C) In vitro-translated, [^{35}S]-labeled GST-fusions of PML fragments or GST were tested for interaction with luciferase as described in (A).

Figure S4. Modification of misfolded proteins by SUMO2/3 (related to Figures 3 and 4).

(**A**) HeLa cells were transfected with FLAG-Atxn1 82Q or FLAG-Atxn1 82Q (5KR) and were treated with or without MG132. FLAG-Atxn1 82Q and FLAG-Atxn1 82Q (5KR) were isolated by d-IP, and their SUMO2/3 modification was analyzed by Western blot.

(**B**) HeLa cells were transfected without or with GFP-TDP-43 and treated with vehicle (DMSO) (-) or MG132 (+). d-IP was performed using an anti-GFP antibody or a control antibody. d-IP products were analyzed by Western blot.

(**C**) HeLa cells were transfected with nFluc-GFP, nFlucSM-GFP, and nFlucSM-GFP (each was also N-terminally tagged with the FLAG epitope) and treated with or without MG132. nFluc proteins were isolated by d-IP. The whole cell lysates (WCL) and IP products were analyzed by Western blot. Note that the difference between the SUMO2/3 modifications of WT luciferase versus SM/DM luciferase (top, lanes 1-3) was not due to a change in the overall SUMO2/3 conjugation in the WCL (bottom).

(**D**) Atxn1 82Q-GFP was expressed in HeLa cells pre-treated with control (Ctrl), SUMO2/3, or SUMO1 siRNA. Cell lysates were analyzed by Western blot.

(**E** and **F**) HeLa cells were treated with control (Ctrl) siRNA, SUMO2/3 siRNA, or SUMO1 siRNA (E), or treated with these siRNAs and then transfected with GFP (F). Cell lysates were analyzed by Western blot.

(**G**) PML and PML M6 proteins used for *in vitro* SUMOylation assay. FLAG-PML and FLAG-PML M6 were expressed in 293T cells and purified by anti-FLAG (M2) beads. The proteins were analyzed by Coomassie staining along with BSA standards (left) and by Western blot (right). The two additional bands (arrowheads) presented in both PML and PML M6 lanes (left) were determined to be PML fragments based on both Western

blot (right) and by mass spectrometry analysis. A schematic representation of M6 mutant is shown at the bottom. *: Point mutations as described in the Experimental Procedures.

Figure S5. RNF4 promotes degradation of misfolded proteins (related to Figure 5)

(**A**) Representative fluorescence images of HeLa cells expressing Atxn1 82Q-GFP alone or together with RNF4. Scale bar: 20 μm. Images are from the same experiment as that shown in Figure 1B.

(**B**) The half-life of Atxn1 82Q-GFP in HeLa cells with and without RNF4 overexpression. Samples are from the same experiments as those shown in Figure 1F.

(**C**) HeLa cells were transfected with control siRNA (-), RNF4 siRNA alone, or RNF4 siRNA plus an siRNA-resistant RNF4. Cell lysates were analyzed by Western blot.

(**D**) FLAG-Atxn1 82Q was expressed in HeLa cells that were pre-treated with control siRNA and the indicated RNF4 siRNA. FLAG-Atxn1 82Q was isolated by d-IP with anti-FLAG M2 beads. WCL and IP products were analyzed by Western blot with indicated antibodies.

(**E**) HeLa cells expressing both Atxn1 82Q-GFP and FLAG-RNF4 were treated with vehicle (DMSO) or MG132. Exogenous (Exo.) RNF4 was detected anti-FLAG antibody. In control cells treated with DMSO, exogenous RNF4 showed partial co-localization with Atxn1 82Q-GFP aggregates. Upon MG132 treatment, complete co-localization of exogenous RNF4 with Atxn1 82Q aggregates was observed in 100% of cells. Scale bar: 10 μm.

(**F**) Western blot analysis of HeLa cells transfected with GFP-TDP-43 alone or together with increasing amounts of RNF4.

(**G**) GFP-TDP-43 was expressed in cells pre-treated with a control siRNA (-) or the indicated RNF4 siRNA. 500 cells were counted in each experiment. Percentages of cells with GFP-TDP-43 foci are shown.

(**H**) HeLa cells treated with RNF4 siRNA were transfected with GFP-TDP-43. Cells were stained with an anti-RNF4 antibody (red) and DAPI (blue). Note that TDP-43 formed aggregates in a cell in which RNF4 was knocked down (filled arrowhead), but was diffused in a control cell (open arrowhead).

(**I**) HeLa cells were transfected with GFP-TDP-43 and treated with MG132. Endogenous RNF4 was immunostained with anti-RNF4 antibody (red). Note that RNF4 also formed nuclear foci in cells with no TDP-43 (*e*-*h*).

Figure S6. SUMO2/3 are involved in RNF4-mediated degradation of Atxn1 82Q (related to Figure 6)

(**A**) Atxn1 82Q-GFP and/or RNF4 were expressed in HeLa cells pre-treated with control siRNA, SUMO2/3 siRNA, and SUMO1 siRNA. Cell lysates were analyzed by Western blot.

(**B**) U2OS cells stably expressing GFP-SUMO2 were transfected first with the indicated RNF4 siRNAs or a control siRNA (-) and then with FLAG-Atxn1 82Q. The percentages of transfected cells with GFP-SUMO2-positive Atxn1 82Q aggregates are shown (mean $\pm$ SD, n=3). In each experiment, 200 cells were counted. Representative images of the transfected cells are shown on the right. GFP-SUMO2 does not form aggregated structure in cells without Atxn1 82Q expression.

(**C**) Schematic representation of wild-type and mutant RNF4 proteins. The SUMO-interaction motifs (SIMs) 1 to 4 and the RING domain are shown. *: Point mutations as described in the Experimental Procedures.

(D and **E)** Purified recombinant GST fusions of rat (r) RNF4 and RNF4 CS1 (D) or human RNF4 and RNF4 SIM^{m} (E) were incubated with ubiquitin E1, E2 (UbcH5a), and ubiquitin (Ub) as indicated, plus Mg^{2+}-ATP. The reaction mixtures were analyzed by Western blot using an anti-GST antibody.

(**F**) Expression of Atxn1 82Q-GFP in cells treated with the indicated combinations of control, PML, and RNF4 siRNAs as indicated. Cell lysates were analyzed by Western blot.

Figure S7. PML deficiency reduces arborization of Purkinje cell dendrites but do not result in aggregates in Purkinje cells (related to Figure 7)

(**A**) Midsagittal cerebellar sections of 12-week-old mice were stained with an antibody against the Purkinje cell-specific protein calbindin. Fluorescence intensity was plotted from a rectangular area from the preculminate fissures (n = 2 mice for $PML^{+/+}$, and n = 3 mice for all the other genotypes). $PML^{-/-}$ mice showed significant loss of dendritic arborization compared to $PML^{+/+}$ mice (ANOVA, p = 0.031).

(**B**) Representative confocal images of calbindin immunofluorescence. Scale bar: 100 μm.

(**C**) Quantitation of Purkinje cell density in 12-week $PML^{+/+}$, $PML^{+/-}$ and $PML^{-/-}$ mice with and without $Atxn1^{tg/-}$, graphed as the average number of soma per 1 mm length (means ± SEM, n = 3 mice/genotype).

(**D**) Immunohistochemical staining of the cerebellar cortex sections from 12-week-old $PML^{+/+}$ and $PML^{-/-}$ mice without $Atxn1^{tg/-}$. The sections were stained with an anti-ubiquitin antibody and counterstained with hematoxylin. Scale bar: 50 μm. Note that no ubiquitin positive aggregates were detected in those sections. The stained sections of $PML^{+/+}$:$Atxn1^{tg/-}$ and $PML^{-/-}$:$Atxn1^{tg/-}$ mice are shown in Figure 7G.

Supplemental Experimental Procedures

Plasmids

All proteins are of human origin unless otherwise indicated. Plasmids for expressing the following proteins in mammalian cells were made in pRK5 by PCR, and each was fused with HA, FLAG, or 6xHis tag, or GST or GFP protein at the NH_2- or COOH-terminus as indicated: FLAG-PML mutants (isoform IV unless otherwise indicated); GST-PML; Atxn1 82Q-GFP, HA-Atxn1 82Q-FLAG, FLAG-Atxn1 82Q; HA-Httex1p 97QP and HA-Httex1p 97QP(KR); FLAG-nFluc-GFP, FLAG-nFlucSM-GFP, and FLAG-nFlucDM-GFP; HA-RNF4, HA-RNF4 SIM^m, HA-RNF4-FLAG, and HA-RNF4 SIM^m-FLAG; and HA-SUMO2 KR. Atxn1 82Q plasmids were made based on the FLAG-Atxn1 82Q/pcDNA plasmid provided by H. Orr (Riley et al., 2005); Httex1p 97QP and Httex1p 97QP(KR) (in which K6, K9, and K15 were changed to Arg) based on the corresponding ones provided by J. L. March (Steffan et al., 2004); and nFluc plasmids based on those provided by S. Raychaudhuri (Gupta et al., 2011). Each nFluc protein was fused to the SV40 nuclear localization signal (PKKKRKV) at the NH_2-terminus and to GFP at the COOH-terminus. In FlucDM, R188 and R261 were changed to Glu; In FlucSM, R188 was changed to Glu (Gupta et al., 2011). The template for PCR amplification of RNF4 was purchased from Open Biosystems (gene accession number: NM002938). In RNF4 $SIM^{m,}$ the following resides within SIMs were changed to Ala: I36, L38, and V39 (SIM1); I46, V47, and L49 (SIM2); V57, V58, and V59 (SIM3); and V67, V68, I69 and V70 (SIM4). In SUMO2 KR, the internal SUMOylation consensus site Lys11 was mutated to Arg.

For bacterial expression, GST fusions of Htt 25Q, Htt 103Q, Htt 52Q, Htt 52Q cc-, PML CC-FLAG, RNF4, and RNF4 SIM^m were constructed in pGEX-1ZT, a derivative of pGEX-1λT with additional cloning sites. Htt 25Q, Htt 52Q and Htt 103Q contained the Htt amino acids 1-17 followed by a polyQ stretch of the indicated length (Krobitsch and Lindquist, 2000). Htt 52Q and Htt 52Q cc- cDNAs were assembled by joining synthetic oligos. FLAG-PML F12 (571-633)-6xHis was constructed in pET28a. All plasmids generated for this study were confirmed by DNA sequencing.

The following plasmids were previously described: FLAG-PML, FLAG-PML M6 (which had the C57S, C60S, C129A, C132A, C189A, and H194A mutations), 6xHis-SUMO1, and 6xHis-SUMO2 (Chu and Yang, 2011); FLAG-Atxn1 82Q and FLAG-Atxn1 30Q (Riley et al., 2005); luciferase-6xHis (a *Photinus pyralis* luciferase variant) (Sharma et al., 2010); GST-rRNF4 (where "r" denotes rat origin, same below), GST-rRNF4 CS1 (in which C136 and C139 were changed to Ser), FLAG-rRNF4, and FLAG-rRNF4 CS (in which C136, C139, C177, and C180 were changed to Ser) (Hakli et al., 2004); and PML isoforms I, II, III, IV, and VI (used in Figure S1A) (Xu et al., 2005).

siRNAs

PML and RNF4 siRNAs were purchased from Qiagen, and the sense strand sequences were: PML#4, CTCCAAGATCTAAACCGAGAA; PML#9, CACCCGCAAGACCAACAACAT; RNF4#5, CCCTGTTTCCTAAGAACGAAA; RNF4#6, TAGGCCGAGCTTTGCGGGAAA; RNF4#8, AAGACTGTTTCGAAACCAACA. RNF4 was knocked down with either siRNAs

individually or in combination at an equal molar ratio. SUMO1 siRNA (Thermo Scientific, siGENOME SMARTpool M-016005-03-0005) was a pool of 4 target-specific siRNA duplexes. The sense strand sequences were: TCAAGAAACUCAAAGAATC, GACAGGGTGTTCCAATGAA, GGTTTCTCTTTGAGGGTCA, and GAATAAATGGGCATGCCAA. SUMO2/3 siRNAs (Santa Cruz sc-37167) was a pool of three different siRNA duplexes, and sense strand sequences were CCCAUUCCUUUAUUGUACA, CAGAGAAUGACCACAUCAA, and CAGUUAUGUUGUCGUGUAU.

Cell culture and transfection

HeLa cells (from ATCC) and U2OS cells expressing GFP-SUMO2 or GFP-SUMO3 (Mukhopadhyay et al., 2006) were maintained in standard culture conditions. DNA plasmids were transfected into cells using Lipofectamine 2000. When PML and Atxn1 were co-transfected, either FLAG-PML plus Atxn1 82Q/30Q-GFP or HA-PML plus FLAG-Atxn1 82Q/30Q was used. HA-RNF4 and HA-RNF4-FLAG plasmids were used for testing protein expression and cellular localization, respectively.

siRNAs using Lipofectamine 2000 or RNAiMAX (Invitrogen), according to the manufacturer's instructions. For knockdown experiments, two rounds of siRNA transfection were performed on consecutive days. When both DNA and siRNA were transfected, DNA was transfected 4-6 h after treatment with combined RNF4 siRNAs, and a day after treatment with other siRNAs. MG132 (Sigma) was added 24 h after the last transfection at 7.5-10 μM (final concentration) for 4-5 h.

Generation of RNF4 shRNA stable cell lines

shRNA against human RNF4, cloned into pLKO.1, was obtained from Thermo Scientific. The antisense sequence of shRNF4 is TGGCGTTTCTGGGAGTATGGG (TRCN0000017054). For lentiviral production, 293T cells were transfected with lentiviral vectors, Gag helper plasmid, Rev helper plasmid, and VSVG helper plasmid. Virus-containing media was collected at 48 h and 72 h and spun for 5 min at 100 g. HeLa cells were transduced using virus-containing supernatant with polybrene and selected with puromycin. The pLKO.1 vector was used to create control stable cells.

Cell lysate fractionation, filter retardation assay, and Western blot

Samples were prepared as described with modifications (Janer et al., 2006). Cells were harvested and lysed for 30 min on ice in buffer containing 50 mM Tris, pH 8.8, 100 mM NaCl, 5 mM $MgCl_2$, 0.5% NP-40, 2 mM DTT, 250 IU/ml benzonase (Sigma), 1 mM PMSF, 1x complete protease cocktail (Roche), and 20 mM N-Ethylmaleimide (NEM; Sigma). Protein concentrations were determined by Bradford assay (Bio-Rad Labs). The whole cell lysates were centrifuged at 13,000 rpm for 15 min at 4 °C. The supernatant, containing NP-40-soluble (NS) proteins, was analyzed by SDS-PAGE. The pellet was re-suspended in the pellet buffer (20 mM Tris, pH 8.0, 15 mM $MgCl_2$, 2 mM DTT, 250 IU/ml benzonase, 1 mM PMSF, 1X complete protease cocktail, and 20 mM NEM) and incubated for 30 min on ice. The pellet fraction was boiled in 2% SDS, 50 mM DTT. One portion of the boiled pellet fraction was resolved by SDS-PAGE, and proteins entering the gel (SDS-soluble, SS) were detected by Western blot. The other portion was applied to a membrane filter with 0.2 μm pore size as previously described (Wanker et al., 1999),

and the SDS-resistant (SR) aggregates retained on the filter was analyzed by immunoblotting.

Primary antibodies against the following proteins were used for Western blot with product information and dilutions indicated: PML (rabbit, H-238, 1:1,000 and goat, N-19, 1:500), ubiquitin (mouse, P4D1, 1:10,000), and HA (rabbit, Y-11, 1:500) (Santa Cruz Biotechnology); FLAG (mouse, M2, 1:7,500), actin (rabbit, 1:10,000), and β-tubulin (mouse, 1:5,000) (Sigma); GFP (mouse, 1:4,000) (Clonetech); GST (goat, 1:1000, GE Healthcare Life Sciences); SUMO1 (mouse, 1:500, Invitrogen); SUMO2/3 (rabbit, 1:250, Abgent); HA (for transfected HA-RNF4) (rat, 3F10, horseradish peroxidase or HRP-conjugated, 1:10,000) (Roche); RNF4 (mouse, 1:500, Abnova, and a mouse monocolonal antibody developed by Abmart using antigen peptide DLTHNDSVVI, 1:1,000). Transfected FLAG-PML was detected by anti-FLAG antibody, and transfected HA-PML and HA-RNF4 were detected by HA antibody.

The secondary antibodies were either conjugated to HRP (Santa Cruz Biotechnology), or labeled with IRD Fluor 800 or IRD Fluor 680 (LI-COR, Inc.). Western blots were developed using ECL reagents and analyzed using ImageJ, or scanned with the Odyssey infrared imaging system, and analyzed using Image Studio Lite (LI-COR, Inc.).

Immunofluorescence of cultured cells

Cells cultured on coverslips were fixed with 4% paraformaldehyde for 15 min, permeabilized with 0.2% Triton X-100 for 15 min, blocked with 1% BSA, and incubated with antibodies as indicated. Cells were mounted with medium containing DAPI (for

DNA detection) (Vector Labs), and the images were acquired with a Nikon Eclipse E800 or Olympus IX81 microscope. The following primary antibodies were used with product information and concentrations indicated: PML (rabbit, H-238 and mouse, PG-M3, 1:100), RNF4 (goat, C-15, 1:25) (Santa Cruz Biotechnology), and FLAG (for transfected FLAG-PML and HA-RNF4-FLAG) (mouse, M2, 1:2,000) (Sigma). Secondary antibodies were FITC-conjugated anti-mouse, anti-rabbit (Zymed), and anti-goat (Invitrogen) IgGs; Texas Red-conjugated anti-mouse and anti-rabbit IgGs (Vector labs); and Rhodamine Red-X conjugated anti-goat (Jackson ImmunoResearch Labs).

For quantification of Atxn1 82Q, Httex1p 97QP, and SUMO2-positive Atxn1 82Q aggregates, approximately 400, 500, and 200 cells, respectively, from ten or more randomly selected fields were examined. The sizes of Atxn1 82Q inclusions were measured using ImageJ, and cells were categorized based on the largest inclusion in cells. *P*-value for the proportions of cells with aggregates of various sizes in the presence and the absence of PML was calculated using a chi-squared test. For cells transfected with Httex1p 97QP, approximately 30% of them had either cytoplasmic or nuclear aggregates.

Assays of protein half-life

For pulse-chase analysis, HeLa cells were transfected with FLAG-Atxn1 82Q alone or together with a moderate amount of PML. 17 h after transfection, cells were cultured in Met and Cys-free DMEM medium for 30 min, and then pulse labeled for 30 min with [^{35}S]Met and [^{35}S]Cys (100 μCi/ml each). Afterwards, cells were rinsed twice with PBS and chased in DMEM with 10% FBS for 0-18 h. Cells were lysed in IP-lysis buffer (50 mM HEPES, pH 7.5, 150 mM NaCl, 0.5% NP-40, and 2 mM DTT) containing 2% SDS

and 50 mM DTT, and boiled at 95 °C for 10 min. The whole cell lysates were centrifuged at 13,000 rpm for 15 min. The supernatants were diluted 20-fold in IP-lysis buffer and incubated with anti-FLAG M2 beads at 4 °C overnight. The beads were sequentially washed with IP lysis buffer with additional 0, 0.5 M, and 1 M KCl, and boiled in a 2% SDS sample buffer. Samples were resolved by SDS-PAGE and analyzed by autoradiography. To better compare the half-life of Atxn1 82Q under different conditions, exposures with similar signal intensity at 0 h were presented.

For cycloheximide (CHX) treatment of Atxn1 82Q-transfected cells, 150 μg/ml CHX was added to cell culture medium 4-5 h after transfection. Cells were harvested and snap-frozen on dry ice at indicated time points, lysed, and fractioned for Western blot analysis. For CHX treatment of nFlucDM-transfected cells, 50 μg/ml CHX was added to cell culture medium 17 h after transfection. Cells were harvested at indicated time points, and whole cell lysates were used for Western blot analysis.

Quantitative RT-PCR analysis

Total RNA was extracted using TRIzol (Invitrogen). cDNA synthesis was carried out by reverse transcription of total RNA using the First Strand cDNA Synthesis Kit (Marligen Biosciences). A Taqman Gene Expression Assay (Applied Biosystems) with human Atxn1 (Hs00165656_m1) and 18s rRNA (4333760F) primers/probe sets were used for qPCR analysis.

Protein purification

FLAG-PML, FLAG-PML M6, and FLAG-Atxn1 82Q-HA were expressed in 293T cells and purified by anti-FLAG M2 beads (Sigma) as previously described (Tang et al., 2006; Tang et al., 2004) with modifications. Cells were lysed in IP-lysis buffer (50mM Tris, pH 7.5, 150 mM NaCl, 0.5% Triton X-100, 0.5% NP-40 and 2 mM DTT) supplemented with 1 mM PMSF, and 1x complete protease cocktail. For PML purification, IP-lysis buffer was also supplemented with 20 μM $ZnCl_2$. The lysates were centrifuged at 13,000 rpm for 15 min. Supernatants were incubated with anti-FLAG M2 beads at 4°C for 4 h to overnight. M2 beads were sequentially washed with IP lysis buffers containing 0, 0.5, and 1 M KCl, and with an elution buffer (50 mM Tris, pH 7.5, 150 mM NaCl, and 2 mM DTT). The bound proteins were eluted in the elution buffer containing 0.1-0.3 mg/ml 3xFLAG peptide (Sigma). The major additional bands observed in the FLAG-PML and FLAG-PML M6 preps were derived from PML based on both Western blot and mass spectrometry analyses (Figure S4G).

GST fusion of PML was expressed in 293T cells and purified using glutathione-Sepharose™ 4B beads (GE Healthcare Life Sciences) with similar lysis and wash conditions as described above. GST fusions of rRNF4, rRNF4 CS1, RNF4, and RNF4 SIM^m were expressed in *Escherichia coli* BL21 DE3 or Rosetta 2 (EMD Chemicals) and purified as previously described (Hakli et al., 2001). The bacteria were grown at 37°C to A_{600nm} = 0.6 - 0.8, and were induced for protein expression with 0.3 mM IPTG for 3 h at 30°C. GST-tagged proteins were purified with glutathione beads. GST and GST fusions of Htt 25Q, Htt 103Q were purified similarly except that 0.1 mM IPTG was used for inducing protein expression. The bound proteins were eluted in the elution buffer containing 30 mM glutathione (Sigma).

Luciferase-6xHis was expressed in BL21 DE3 as previously described (Sharma et al., 2010). To generate immobilized native luciferase, Luc (N), Ni-NTA beads (Qiagen) were incubated with bacterial lysates and washed according to the manufacturer's instructions. Denatured luciferase, Luc (D), was generated by treating immobilized Luc (N) with 8 M urea for 5 min. A luciferase activity assay showed that only 0.2% of enzymatic activity remained after urea treatment. For control beads, lysates from bacteria expressing no luciferase were incubated with Ni-NTA beads in parallel.

To generate PML mutants used for luciferase peptide scans, FLAG-PML F12 (571-633)-6xHis and GST-PML CC-FLAG were expressed in BL21 DE cells at room temperature with 0.1 mM IPTG induction for 3 h and 1 h, respectively. Flag-PML F12 (571-633)-6xHis was purified first using M2 beads and the FLAG peptide elution, and was subjected to a second purification using Ni-NTA beads, according to the manufacturer's instructions. To generate the PML CC domain, a TEV protease cleavage site was introduced between GST and PML CC. The GST-PML CC-FLAG conjugated glutathione beads were incubated with TEV protease (Sigma) according to the manufacturer's instructions to release PML CC-FLAG from the GST moiety (and from the beads). PML CC-FLAG used for pull-down assay was generated by incubating the purified PML CC-FLAG proteins with M2 beads and washed as described above.

Pull-Down Assays

For FLAG pull-down assays, FLAG-PML, FLAG-GFP and PML CC-FLAG bound to anti-FLAG M2 beads were prepared as described above. Purified GST-Htt 25Q, GST-Htt 103Q, GST-Htt 52Q or GST-Htt 52Q cc- were centrifuged at 13,000 rpm for 15 min to

remove any aggregated proteins. FLAG-PML (2.5 μg) or FLAG-GFP (1.1 μg) at comparable molarity was incubated with GST-Htt 25Q or GST-Htt 103Q (2.5 μg each) in the absence or presence of Hsp70 (2.5 μg) and Hsp40 (1.4 μg) (Enzo Life Sciences) in a final volume of 200 μl assay buffer (50 mM Tris, pH 7.5, 150 mM NaCl, and 2 mM DTT, 0.5% NP-40) for 2 h at 4 °C. The beads were washed three times with IP-lysis buffer in Compact Reaction Columns (Affymetrix/USB) and boiled in 2% SDS sample buffer. Samples were analyzed by Western blot. The PML CC pull-down assay was performed similarly, except M2 beads containing 1.6 μg PML CC-FLAG or control M2 beads were incubated with 5 μg GST or GST-Htt proteins.

For GST pull-down assay, 2 μg each of GST, GST-Htt 25Q, and GST-Htt 103Q proteins that bound to glutathione-Sepharose™ 4B beads were incubated with 400 μg lysates from 293T cells expressing FLAG-PML protein at 4 °C for 4 h. The beads were washed three times with IP-lysis buffer in Compact Reaction Columns and boiled in 2% SDS sample buffer. Samples were analyzed by Western blot. For detecting the interaction between PML mutants and Htt**,** [^{35}S]Met-labeled full-length and mutant PML proteins were generated using the SP6 Coupled Transcription/Translation System (Promega) and incubated with GST, GST-25Q and GST-Htt 103Q that bound to beads in 150 μl IP-lysis buffer at 4 °C overnight. Beads were washed and boiled as described above. Input and pull-down samples were analyzed by autoradiography and Coomassie blue staining. For autoradiography, pull-down samples from the same experiments that were resolved on different gels were subjected to the same exposure time.

For the luciferase pull-down assay, 3 μg of Luc (N) or Luc (D) bound Ni-NTA beads or control beads prepared from an equal amount of bacterial lysate were incubated

with purified GST (1 μg), GST-PML (3 μg) in the absence or presence of Hsp70 (3 μg) and Hsp40 (1.7 μg), or [^{35}S]Met-labeled full-length and mutant PML proteins in 200 μl PBS containing 15 mM Imidazole, 1 mM DTT, 0.5% Triton X-100 and 0.5% NP-40 at 4 °C for 4 h. The beads were washed three times with PBS containing 20 mM Imidazole, 1 mM DTT, 0.5% Triton X-100 and 0.5% NP-40 and boiled. The input and pull-down samples were analyzed as described above.

Screening of cellulose-bound peptides for binding to PML domains

A peptide library (13-mers overlapping by ten amino acids) for *Photinus pyralis* luciferase was prepared by automated spot synthesis (JPT peptide Technologies). The peptide array membrane was blocked with Odyssey Blocking buffer (LI-COR, Inc) and incubated with FLAG-PML F12(571-633)-HisX6 or PML F4/CC-FLAG (150 nM each) in TBS-T (50 mM TRIS, pH 8.0, 137 mM NaCl, 2.7 mM KCl, 0.05% Tween and 1 mM DTT) at 4 °C for 2 h. The membrane was washed and blotted with mouse anti-Flag and anti-mouse-HRP antibodies following the manufacturer's instructions. The blots were developed using ECL reagents. Background signal on blots with anti-Flag and anti-mouse-HRP antibodies alone was minimal even at long exposures (data not shown). The peptide array membrane was regenerated according to the manufacturer's protocol.

***In vivo* SUMOylation and ubiquitination assays**

Cells were transfected with FLAG-Atxn1, FLAG-nFluc-GFP, and other expression plasmids as indicated. For the experiments shown in Figure 4A, a SUMO2-expressing plasmid was also used. 24 h after transfection, cells were treated with 7.5 μM MG132 or

DMSO for 5 h or left untreated, and harvested in IP-lysis buffer supplemented with 2% SDS and 50 mM DTT. For denaturing immunoprecipitation (d-IP), cell lysates were boiled at 95°C for 10 min. One aliquot was saved for Western blot analysis. The rest of the lysates were either diluted 20-fold in IP-lysis buffer or passed through a Bio-Spin chromatography column (Bio-Rad) equilibrated with IP-lysis buffer to reduce the SDS concentration. Lysates were then incubated with anti-FLAG (M2) beads at 4°C for 4 h or overnight. The beads were washed as described for FLAG-tagged protein purification, and boiled in 2% SDS sample buffer. Proteins from beads were analyzed by Western blot with anti-FLAG, -SUMO2/3, -SUMO1, -ubiquitin, and other antibodies as indicated. To better compare the levels of ubiquitinated or SUMOylated species, d-IP products containing similar levels of unmodified proteins were often used for Western blot analysis.

***In vitro* SUMOylation assays**

Components for *in vitro* ubiquitination and SUMOylation reactions were purchased from Boston Biochem. *In vitro* SUMOylation assays were performed at 37 °C for 1.5 h in 30 μl reaction buffer (50 mM Tris pH 7.5, 5.0 mM Mg^{2+}-ATP, and 2.5 mM DTT) containing purified HA-Atxn1 82Q-FLAG (600 ng /200 nM), FLAG-PML (for Figure 4D, 50 and 200 ng or 22 and 90 nM; for Figure 4E 100 ng or 45 nM) or FLAG-PML M6 (100 ng or 45 nM), SAE1/SAE2 (125 nM), Ubc9 (1 μM), His-SUMO2 (25 μM), Hsp70 (420 ng / 200 nM), Hsp40 (240 ng/200 nM) and BSA (0.1 μg/ml). The reaction mixtures were denatured by the addition of 30 μl IP-lysis buffer containing 2% SDS and 50 mM DTT and heating at 95°C for 10 min. One aliquot of the heated reaction mixes were saved for

Western blot analysis, and the rest were diluted 20-fold in IP-lysis buffer without SDS. HA-Atxn1-FLAG was immunoprecipitated by anti-HA beads (Roche) and analyzed for SUMO2/3 modification using anti-SUMO2/3 antibodies.

***In vitro* ubiquitination assays**

In vitro assays for RNF4 self-ubiquitination were performed at 37°C for 1 h in 10 μl reaction buffer (50 mM Tris pH 7.5 and 2.5 mM DTT) containing purified GST-RNF4 protein (250 ng/530 nM), UBE1 (125 nM), UbcH5a (625 nM), ubiquitin (2.5 μg/30 μM), and Mg^{2+}-ATP (2.5 mM). The reaction mixtures were heated at 95°C for 10 min and analyzed by Western blot.

For *in vitro* ubiquitination of SUMOylated Atxn1 82Q, a mix of SUMOylated and unmodified Atxn1 82Q proteins was prepared as ubiquitination reaction substrate. M2 beads conjugated with FLAG-Atxn1 82Q-HA (1.5 μg/300 nM) and control M2 beads were mixed with 0.75 μM SAE1/SAE2, 12.5 μM Ubc9, 125 μM His-SUMO2, and 2.5 mM DTT in a total volume of 50 μl of Mg^{2+}-ATP-Energy Regeneration Solution containing 5 mM ATP (Boston Biochem). To achieve sufficient Atxn1 82Q SUMOylation, the reaction was performed at 37 °C for 24 h, and the reaction buffer was replaced after 12 h. Beads were then washed sequentially with IP-lysis buffer with additional 0, 0.5, and 1 M KCl and with ubiquitination reaction buffer (50 mM Tris pH 7.5 and 150 mM NaCl) (Tang et al., 2006).

Atxn1 82Q beads and control beads were then incubated at 37 °C for 1 h with ubiquitination reaction mixes in 20 μl volume containing GST-rRNF4 (0, 40, 160 and 500 ng, or 0, 43, 170, and 530 nM), UBE1 (100 nM), UbcH5a (500 nM), ubiquitin (5

μg/30 μM), and Mg^{2+}-ATP (2.5 mM) in reaction buffer (50 mM Tris-HCl pH 7.5, 150 mM NaCl, and 2.5 mM DTT). Afterwards, beads were separated from the supernatant and washed with IP-lysis buffer. Atxn1 82Q was denatured and released from the beads by the addition of IP-lysis buffer containing 2% SDS and 50 mM DTT and heat at 95°C for 10 min. After dilution, Atxn1 82Q was immunoprecipitated with M2 beads. The IP products and the supernatant from the reaction were analyzed by Western blot.

Mouse breeding and genotyping

The heterozygous B05 transgenic mice (*Atxn1*$^{tg/-}$), which harbor the human *SCA1*-coding region with 82 CAG repeats driven by a Purkinje cell-specific promoter element, were kindly provided by H. T. Orr (Burright et al., 1995). *PML*$^{-/-}$ mice were kindly provided by P.P. Pandolfi (Wang et al., 1998). *Atxn1*$^{tg/-}$ mice (on FVB background) were mated with *PML*$^{-/-}$ (on 129Sv background). *PML*$^{+/-}$*:Atxn1*$^{tg/-}$ mice from the F1 generation were mated with *PML*$^{-/-}$ or *PML*$^{+/+}$ to generate mice used for Rotarod tests and pathology. The mating scheme did not affect the Rotarod performance, formation of aggregates, molecular layer thickness, or dendritic arborization of the F2 generation of *PML*$^{+/-}$ or *PML*$^{+/-}$*:Atxn1*$^{tg/-}$ mice. The mouse genotype was determined by PCR either as described (Burright et al., 1995) (for *Atxn1*) or according to suggestions by the NCI Mouse Repository (for *PML*). All animal experiments were performed in accordance with relevant guidelines and regulations and were approved by the University of Pennsylvania Institutional Animal Care and Use Committee (IACUC).

Accelerating Rotarod test

An accelerating Rotarod apparatus (47600, Ugo Basile, Italy) was used to measure motor coordination and balance. Only naïve animals were used. Each animal was given three trials per day for four consecutive days, with a 1 h rest between trials. For each trial, mice was placed on the Rotarod with increasing speed, from 4-80 rpm, over 10 min. Their latency to fall off the Rotarod (in seconds) was recorded.

Immunostaining and pathological analysis of mouse cerebellum

Immunohistochemistry and immunofluorescence were performed as previously described with modifications (Duda et al., 2000; Emmer et al., 2011). Paraffin-embedded cerebella were cut into 10-μm sections. For molecular layer measurements, three haematoxylin stained midsagittal sections with 100 μm intervals were analyzed per mouse. Twenty measurements at the primary fissure for each section were averaged.

To quantify Purkinje cell dendritic arborization, midsagittal sections of cerebella were stained with an antibody against the Purkinje cell-specific protein calbindin (mouse, CB-955, 1:250; Sigma). Twenty 0.5 μm optical sections were accumulated with Leica SP5 II laser scanning confocal microscope. The brightest continuous 12 sections (6 μm) were projected for maximum intensity. The fluorescence intensity profile from the same region of preculminate fissure was plotted using ImageJ.

To quantify Purkinje cells, midsagittal sections were stained with anti-calbindin antibody and comparable regions were used for cell counting. The length of the Purkinje cell layer was measured by drawing segmented line along Purkinje cell soma center using ImageJ. For each mouse, 350 – 900 neurons along approximately 30 mm were measured.

The Purkinje cell density was determined by dividing the number of cells by the length of Purkinje cell layer.

To determine the number of Purkinje cells with aggregates, midsagittal sections were stained with anti-ubiquitin (mouse, Ubi-1, MAB1510, 1:2,000; Millipore) antibody. 300 cells or more were counted from the same brain regions per mouse. Images were taken using an Olympus BX51 microscope mounted with a DP71 Olympus digital camera.

Four mice per genotype were used for counting Purkinje cells of 1-year-old mice, two $PML^{+/+}$ mice per genotype for quantification of dendritic arborization, and three mice per genotype for the rest of the studies.

Statistical analysis

The numbers of cells with aggregates were analyzed by chi-squared test and Student's t-test when appropriate. The behavioral scores and cerebellar pathology were analyzed by two-way ANOVA with repeated measurements and Student's t-test. All the data were analyzed using Prism5 software or Microsoft Excel 2008.

Supplemental References

Burright, E.N., Clark, H.B., Servadio, A., Matilla, T., Feddersen, R.M., Yunis, W.S., Duvick, L.A., Zoghbi, H.Y., and Orr, H.T. (1995). SCA1 transgenic mice: a model for neurodegeneration caused by an expanded CAG trinucleotide repeat. Cell *82*, 937-948.

Duda, J.E., Giasson, B.I., Gur, T.L., Montine, T.J., Robertson, D., Biaggioni, I., Hurtig, H.I., Stern, M.B., Gollomp, S.M., Grossman, M.*, et al.* (2000). Immunohistochemical and biochemical studies demonstrate a distinct profile of alpha-synuclein permutations in multiple system atrophy. J Neuropathol Exp Neurol *59*, 830-841.

Emmer, K.L., Waxman, E.A., Covy, J.P., and Giasson, B.I. (2011). E46K human alpha-synuclein transgenic mice develop Lewy-like and tau pathology associated with age-dependent, detrimental motor impairment. J Biol Chem *286*, 35104-35118.

Gupta, R., Kasturi, P., Bracher, A., Loew, C., Zheng, M., Villella, A., Garza, D., Hartl, F.U., and Raychaudhuri, S. (2011). Firefly luciferase mutants as sensors of proteome stress. Nat Methods *8*, 879-884.

Hakli, M., Karvonen, U., Janne, O.A., and Palvimo, J.J. (2001). The RING finger protein SNURF is a bifunctional protein possessing DNA binding activity. J Biol Chem *276*, 23653-23660.

Hakli, M., Lorick, K.L., Weissman, A.M., Janne, O.A., and Palvimo, J.J. (2004). Transcriptional coregulator SNURF (RNF4) possesses ubiquitin E3 ligase activity. FEBS Lett *560*, 56-62.

Krobitsch, S., and Lindquist, S. (2000). Aggregation of huntingtin in yeast varies with the length of the polyglutamine expansion and the expression of chaperone proteins. Proc Natl Acad Sci U S A *97*, 1589-1594.

Mukhopadhyay, D., Ayaydin, F., Kolli, N., Tan, S.H., Anan, T., Kametaka, A., Azuma, Y., Wilkinson, K.D., and Dasso, M. (2006). SUSP1 antagonizes formation of highly SUMO2/3-conjugated species. J Cell Biol *174*, 939-949.

Sharma, S.K., De los Rios, P., Christen, P., Lustig, A., and Goloubinoff, P. (2010). The kinetic parameters and energy cost of the Hsp70 chaperone as a polypeptide unfoldase. Nat Chem Biol *6*, 914-920.

Tang, J., Qu, L.K., Zhang, J., Wang, W., Michaelson, J.S., Degenhardt, Y.Y., El-Deiry, W.S., and Yang, X. (2006). Critical role for Daxx in regulating Mdm2. Nat Cell Biol *8*, 855-862.

Tang, J., Wu, S., Liu, H., Stratt, R., Barak, O.G., Shiekhattar, R., Picketts, D.J., and Yang, X. (2004). A novel transcription regulatory complex containing death domain-associated protein and the ATR-X syndrome protein. J Biol Chem *279*, 20369-20377.

Wanker, E.E., Scherzinger, E., Heiser, V., Sittler, A., Eickhoff, H., and Lehrach, H. (1999). Membrane filter assay for detection of amyloid-like polyglutamine-containing protein aggregates. Methods Enzymol *309*, 375-386.

Xu, Z.X., Zou, W.X., Lin, P., and Chang, K.S. (2005). A role for PML3 in centrosome duplication and genome stability. Mol Cell *17*, 721-732.